The Active Role of the Support in Propane ODH over VO_x/CeO_2 Catalysts Studied Using Multiple *Operando* Spectroscopies

Leon Schumacher, Christian Hess*

Eduard-Zintl-Institut für Anorganische und Physikalische Chemie, Technical University Darmstadt, Alarich-Weiss-Str. 8, 64287 Darmstadt, Germany

*Corresponding Author (E-Mail: christian.hess@tu-darmstadt.de)

Abstract

Because of the relevance of supported vanadia catalysts for the oxidative dehydrogenation (ODH) of alcohols and short alkanes, a detailed mechanistic understanding, including the role of the support, is of great importance. In this work, we address the ODH of propane over ceria-supported vanadia (VO_x/CeO_2) catalysts, especially regarding the active participation of ceria and the synergy effect between ceria and vanadia. A combination of *operando* multi-wavelength Raman-, *operando* UV-Vis- and *operando* IR spectroscopy is applied, including the targeted use of different Raman excitation wavelengths to selectively enhance vibrational features through resonance from vanadia (514 nm) and the ceria support (385 nm). Our *operando* results show that surface lattice oxygen from ceria is crucial for the selective oxidation of propane while the structure of vanadia seems to stay unchanged during the reaction. Rather vanadia structures play an indirect role in increasing the overall selectivity of the reaction. The surface oxygen defects of ceria are affected by the interaction with vanadia monomeric species in direct proximity, owing to an irreversible occupancy of the vacancies by vanadia monomers, which slows down the overall oxygen dynamics and thereby decreases the amount of CO_2 produced. Dimeric and oligomeric vanadia species weaken the adsorption of propane onto the ceria surface, further increasing the selectivity. Our mechanistic insights demonstrate the synergy effect between vanadia and ceria in oxidation reactions and provide an experimental basis for a detailed understanding of the role of the support in VO_x/CeO_2 and other supported vanadia catalysts.

TOC graphic

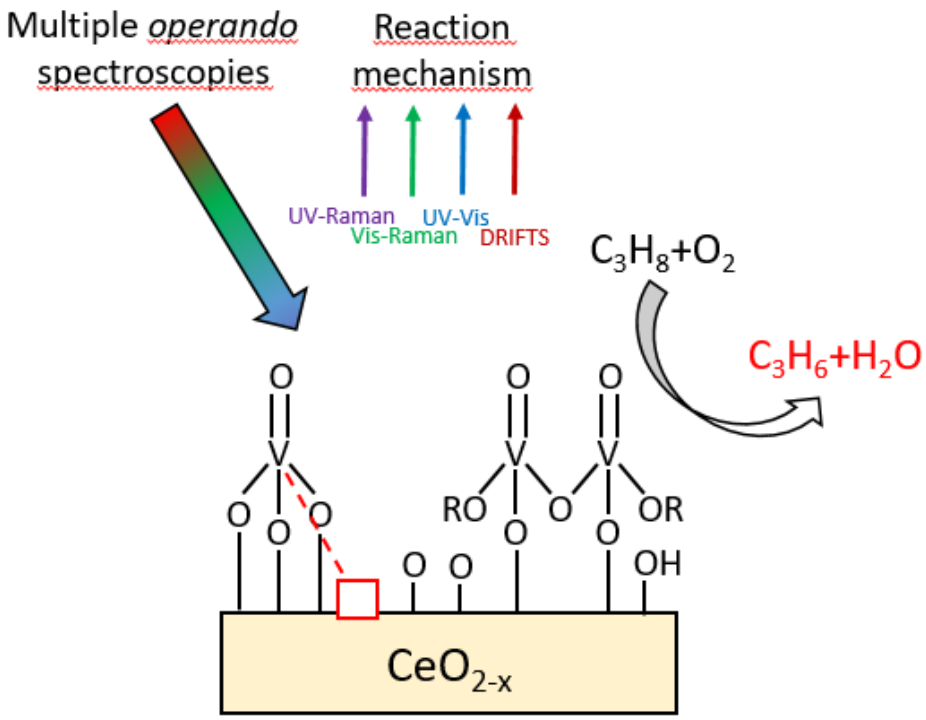

Keywords: oxidative dehydrogenation (ODH), propylene, vanadia, ceria, *operando* spectroscopy, defects, resonance Raman spectroscopy

1. Introduction

Vanadia based catalysts have been shown to be active in the oxidative dehydrogenation (ODH) of alcohols and short-chain alkanes.[1–5] The selective oxidation of propane to propylene is of particular importance due to the increasing demand for propylene to produce polypropylene.[6] The ODH of propane is considered as an alternative/additional way to produce propylene in comparison to conventional processes such as steam cracking or fluid catalytic cracking (FCC).[7] Besides the active phase, the support material also plays an important role with respect to the catalytic activity during propane selective oxidation. Generally, support materials can be classified as inactive (SiO_2, Al_2O_3) or active (TiO_2, ZrO_2, CeO_2), where active materials are proposed to directly participate in the redox cycle.[2,8,9] While vanadia supported on inactive support materials has been studied intensively,[8–15] experimental evidence for the participation of active support materials in selective oxidation reactions is scarce and mostly present for ethane ODH [16,17].

The use of CeO_2 as a support material in combination with vanadia for selective oxidation reactions has attracted considerable attention from both the experimental and theoretical points of view.[2,5,8,9,16–27] The reducibility of the catalyst is regarded as an important factor contributing to the overall reactivity of the system, but direct spectroscopy evidence, for example from *in situ* and *operando* spectroscopy, is still scarce for most reactions,[5,14,16,28–31] especially propane ODH. Previous experimental [16,17,27,32–35] and theoretical[19,22–24,36–40] studies on VO_x/CeO_2 catalysts mainly focused on general properties of the system and the synergy between vanadia and ceria. To this end, it was concluded that the ceria support keeps vanadia in an oxidation state of V^{5+} [16,17,19,27,36] and can actively participate in the reaction through its low defect formation energy.[22,24,37] In the context of propane ODH only a few theoretical studies and even less experimental studies with *operando* spectroscopic evidence are available. Using density functional theory (DFT), Huang et al. investigated possible reaction pathways for propane conversion on the catalyst surface[37] and proposed that propyl adsorption initiated by hydrogen abstraction at ceria surface lattice oxygen (proposed to be the rate-determining step), owing to its low defect formation energy in the proximity of vanadia structures, followed by adsorption of propyl to a V-O-Ce bond. Further possibilities would be a hydrogen abstraction to V-O-Ce or vanadyl bonds and an adsorption of the propane to the ceria surface, since the energy of those structures is very similar.[22,37] In Raman spectroscopic studies on the structural properties

of VO_x/CeO_2 by Wu et al.[35] a synergy effect between ceria defects and vanadia structures was reported, as has been proposed previously for the ODH of ethane and later confirmed using *operando* XANES [16,17,27,28,41]. This was supported by a DFT study by Penschke et al.[22], reporting the structural relaxation of monomeric vanadia structures close to oxygen defects.

In this study, we applied a combination of *operando* multi-wavelength Raman, *operando* UV-Vis, and *operando* DRIFTS (diffuse reflectance infrared Fourier transform spectroscopy) to VO_x/CeO_2 catalysts to address specifically the role of the support material during propane ODH as well as the synergy between the active phase and the ceria support. The use of different Raman excitation wavelengths is crucial to selectively enhance vibrational features from ceria and vanadia, enabling us to unravel the structural dynamics of VO_x/CeO_2 catalysts during propane ODH. While the potential of multi-wavelength Raman spectroscopy has been demonstrated previously for ethanol ODH,[5,14] to the best of our knowledge, such an approach has not been applied to propane ODH over vanadia-containing catalysts such as supported vanadia, supported V_2O_5 or mixed oxide catalysts such as supported $MoVO_x$.[42,43] Combining *operando* Raman, UV-Vis and DRIFT spectroscopy in one study allows the structures of (sub)surface ceria and surface vanadia as well as the presence of adsorbates to be monitored under reaction conditions. Additional mechanistic insight is provided by the dependence of structural properties on vanadium loading.

2. Experimental Section

Catalyst Preparation. Ceria was synthesized as described previously[44] and loaded with vanadia by incipient wetness impregnation. Three different loadings were achieved by mixing 2 g of ceria with 0.5 mL of differently concentrated precursor solutions (1.07 mol/L, 0.51 mol/L, 0.21 mol/L) containing vanadium(V) oxytriisopropoxide (≥ 97%, Sigma Aldrich) and 2-propanol (99.5%, Sigma Aldrich). The samples were then heated to 600 °C at a heating rate of 1.5 °C min^{-1} and calcined at 600 °C for 12 h. The specific surface area of the ceria was determined before the impregnation with vanadia and was determined to be 57 m^2 g^{-1} by nitrogen physisorption experiments and use of the Brunauer–Emmett–Teller (BET) method, yielding vanadia loadings of 2.83 V nm^{-2} (2,12 wt-% V_2O_5), 1.36V nm^{-2} (1,02 wt-% V_2O_5), and 0.57 V/nm^{-2} (0.43 wt-% V_2O_5), respectively. Higher vanadia loadings were not considered due

to the presence of crystallites burying part of the deposited vanadia.[45] The resulting catalyst powders were subsequently pressed at a pressure of 2000 kg m^{-2} for 20 s, ground and then sieved using a combination of sieves with 200 µm and 300 µm opening to obtain 200 – 300 µm particles, suitable for use in a fluidized bed reactor.

UV-Raman Spectroscopy. UV-Raman spectroscopy was performed at an excitation wavelength of 385 nm generated by a laser system based on a Ti:Sa solid state laser pumped by a frequency-doubled Nd:YAG laser (Coherent, Indigo). The fundamental wavelength is frequency doubled to 385 nm using a LiB_3O_5 crystal. The light is focused onto the sample, and the scattered light is collected by a confocal mirror set-up and focused into a triple stage spectrometer (Princeton Instruments, TriVista 555).[45] Finally, the Raman contribution is detected by a charge-coupled device (CCD, 2048×512 pixels) cooled to -120 °C. The spectral resolution of the spectrometer is 1 cm^{-1}. For Raman experiments, 70 mg of catalyst was placed in a CCR 1000 reactor (Linkam Scientific Instruments) equipped with a CaF_2 window (Korth Kristalle GmbH). A fluidized bed reactor was employed to avoid laser-induced damage, allowing the use of a laser power of 9 mW at the location of the sample. Data processing included cosmic ray removal and background subtraction.

Vis-Raman Spectroscopy. Vis-Raman spectroscopy was performed at excitation wavelengths of 514 nm and 532 nm using an argon ion gas laser (Melles Griot) and a frequency-doubled Nd:YAG laser (Cobolt), respectively. The light was focused on to the sample, gathered by an optic fiber and dispersed by a transmission spectrometer (Kaiser Optical, HL5R). The dispersed Raman radiation was subsequently detected by an electronically cooled CCD detector (-40 °C, 1024×256 pixels). The spectral resolution was 5 cm^{-1} with a wavelength stability of better than 0.5 cm^{-1}. For Raman experiments, 70 mg of catalyst was filled into a CCR 1000 reactor (Linkam Scientific Instruments) equipped with a quartz window (Linkam Scientific Instruments). A fluidized bed reactor was employed to avoid laser-induced damage, and for both wavelengths a laser power of 2.5 mW at the sample location was applied. Data analysis of the Raman spectra included cosmic ray removal and an auto new dark correction. Peak fitting analysis was performed for the V=O stretching region of VO_x/CeO_2 samples, fitting five Lorentzian functions to the region between 990 and 1060 cm^{-1} using a Levenberg-Marquardt algorithm implementation in OriginLab 2018.

Diffuse Reflectance UV-Vis Spectroscopy. Diffuse reflectance (DR) UV-Vis spectroscopy was performed on a Jasco V-770 UV-Vis spectrometer. Dehydrated $BaSO_4$ was used as white standard. For each experiment, 90 mg of catalyst was put in the commercially available reaction cell (Praying Mantis High Temperature Reaction Chamber, Harrick Scientific) equipped with transparent quartz glass windows.

Diffuse Reflectance Infrared Fourier Transform Spectroscopy. Diffuse reflectance infrared Fourier transform spectroscopy (DRIFTS) was performed using a Vertex 70 spectrometer (Bruker). A liquid nitrogen-cooled mercury cadmium telluride (MCT) detector was used, operating at a resolution of 1 cm^{-1}. Dehydrated potassium bromide was employed as an infrared transparent sample for the background spectrum. For each experiment, 90 mg of catalyst was placed in the commercially available reaction cell (Praying Mantis High Temperature Reaction Chamber, Harrick Scientific) equipped with transparent KBr windows.

Data processing consisted of background removal by subtracting a baseline formed by 11 anchor points. A background spectrum of the propane gas-phase was recorded using KBr as an infrared transmitting sample. The propane gas phase and the *operando* spectrum were then normalized to the propane gas phase peak at 3000 cm^{-1} and subtracted to remove gas phase contributions from propane. Afterwards, rotational bands from water, formed during the ODH of propane, were removed. Finally, to quantify the adsorbate peaks in the region between 1120 cm^{-1} and 1920 cm^{-1}, the spectrum recorded under oxidizing conditions was subtracted from that recorded under reaction conditions to remove signals caused by the sample itself. Six contributions were identified in the region between 1120 cm^{-1} and 1920 cm^{-1} and four contributions were identified for the region between 2640 cm^{-1} and 2980 cm^{-1}. These were fitted using Lorentzian functions employing the Levenberg-Marquardt algorithm implemented in OriginLab 2018. The spectrum recorded under oxidizing conditions has not been subtracted in Figure 8.

Catalytic Measurements. Catalytic testing was performed by employing a CCR 1000 reaction cell (Linkam Scientific Instruments) in fluidized bed mode using 70 mg of catalyst. Catalyst samples were first dehydrated for 1 h at 400 °C under oxidative conditions (12.5 % oxygen (Westfalen, 5.0) and 87.5 % helium (Westfalen, 5.0), 40 mL_n/min), then cooled to 50 °C, and subsequently exposed to reaction conditions (12.5 % oxygen, 12.5 % propane (Westfalen, 3.5) and 75 % helium, 40mL_n/min). Samples were heated in 50 °C steps up to 600 °C keeping each

temperature for 1 h, while the gas-phase composition was analyzed using gas chromatography (GC, Agilent Technologies 7890B). The GC system consists of two columns – a PoraPlotQ and a Molesieve – as well as a thermal conductivity detector (TCD) and a flame ionization detector (FID) connected through a twelve-way valve. Recording one chromatogram took 29 min; so for each temperature, two chromatograms were measured. The pressure was monitored before and after the GC apparatus in order to be able to correct the detected areas for pressure fluctuations.

***Operando* Measurements.** *Operando* experiments were performed by measuring the catalyst samples first under oxidative conditions (12.5 % oxygen (Westfalen, 5.0) and 87.5 % helium (Westfalen, 5.0), 40 mL_n/min) and then under reactive conditions (12.5 % oxygen, 12.5 % propane (Westfalen, 3.5) and 75 % helium, 40mL_n/min), each at 300 °C in a fluidized bed reactor. For the isotope experiments using propane-d_8, in addition to treatment in oxidative and reactive conditions, measurements in reactive conditions with propane-d_8 were performed (12.5 % oxygen, 12.5 % propane-d_8 (Eurisotope, 98 %) and 75 % helium, 40mL_n/min), after the measurements in reactive conditions using regular propane (propane-h_8). The reaction cells used for *operando* experiments are described in the experimental section of the respective techniques. We verified that the Linkam CCR 1000 reactor produced activity data comparable to that obtained in a fixed bed reactor, by comparing the values for the conversions and selectivities obtained during *operando* experiments with those reported in the literature [9] for similar temperatures and vanadia loadings. As an example, for the *operando* reactor used here, for a loading of 1.36 V/nm^2, at a conversion of 13% a selectivity of 22% was obtained (at 366 °C), compared to a selectivity of 25% at 10% conversion (at 350 °C and 1.5 V/nm^2 loading) in a fixed bed reactor. A scheme of the experimental set-up has been discussed previously by Waleska et al.[45] The penetration depth of the 385 nm radiation (~50-100 nm at 385 nm, ~0.5-1 µm at 514 nm for silicon [46] or ZnO [47]; exact values depend on the actual absorption at the respective wavelength, the material, etc. but values for mixed metal oxides can also be roughly determined [48]) is expected to be significantly lower than that of silicon (<50 nm) owing to the strong absorption of ceria at this wavelength. The temperature of the samples at the surface was determined to be 275 °C for reaction conditions. Characterization of the samples was performed after dehydration at 366 °C for 1 h and cooling back to 25 °C.

3. Results and Discussion

Characterization. Figure 1 presents the DR-UV-Vis spectra of the VO_x/CeO_2 catalyst samples prepared with different vanadium loadings, together with that for bare ceria as a reference. The strong absorption below 400 nm can be attributed to ceria.[35] The features at 262 nm and 330 nm result from band gap absorption of ceria, that is, O 2p → Ce 4f transitions,[49–51] overlapping with the usually observed ligand-to-metal-charge transfer (LMCT) features of vanadia monomers below 300 nm and dimeric species at ~350 nm.[52] Above 400 nm, we observe an increase in absorption with increasing vanadia loading, which has been assigned to LMCT features of oligomeric vanadia species.[52] In the depicted spectra, the excitation wavelengths used for the Raman experiments are marked (385, 514, and 532 nm). An excitation wavelength of 385 nm was chosen because of the significantly higher relative contribution of ceria to the absorption as compared to vanadia, enabling a resonance enhancement for ceria vibrational features. Owing to the low penetration depth at 385 nm excitation, the structural dynamics at the catalyst surface will be measured.[52] As described above, oligomeric vanadia species dominate the absorption behavior at 514 nm (in comparison to 385 nm). Thus, with 514 nm excitation, vanadia-related Raman features can be selectively enhanced due to resonance effects. Laser excitation at 532 nm was chosen to increase the sensitivity towards the characteristic F_{2g} mode as a result of a slightly deeper penetration depth in comparison to 514 nm. In general, excitation at 514 and 532 nm gave similar Raman results. Therefore, only data for either 514 nm or 532 nm excitation will be shown in the following. In conclusion, the multi-wavelength Raman approach enables access to complementary information about VO_x/CeO_2 catalysts.

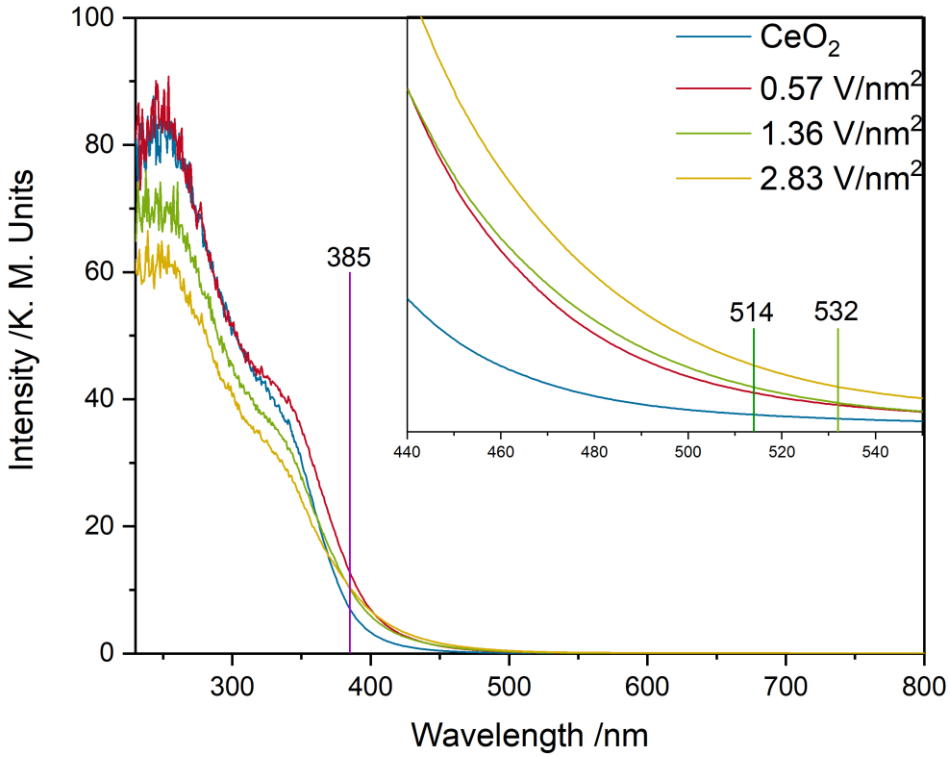

Figure 1: UV-Vis absorption spectra of VO_x/CeO_2 catalysts and bare CeO_2 at 25 °C recorded in 40 mL_n/min helium after dehydration at 366 °C for 1 h (12.5% O_2 in helium, 40mL_n/min). Excitation wavelengths used for Raman spectroscopy are indicated in purple (385 nm), dark green (514 nm), and light green (532 nm). The inset gives an enlarged view of vanadia absorptions in the region between 440 nm and 550 nm.

Figure 2 shows the Raman spectra of the VO_x/CeO_2 catalysts and bare CeO_2 at 385 and 532 nm excitation, which were recorded after dehydration at 366 °C and cooling down to 25 °C in 40 mL_n/min helium. Spectra are normalized to the F_{2g} peak and offset for clarity. As shown at the top of Figure 2, for 385 nm excitation, Raman features appear at 247, 405, 463, 590, 709, 860, 930, 1023, and 1170 cm^{-1}. Ceria-related features include the longitudinal (247 cm^{-1}) and transversal (405 cm^{-1}) Ce-O surface phonons.[53] No specific loading-dependent changes in their intensity is observed. A contribution of the bulk 2TA mode at 250 cm^{-1} to the longitudinal surface phonon cannot be excluded, as discussed previously in the literature.[53]

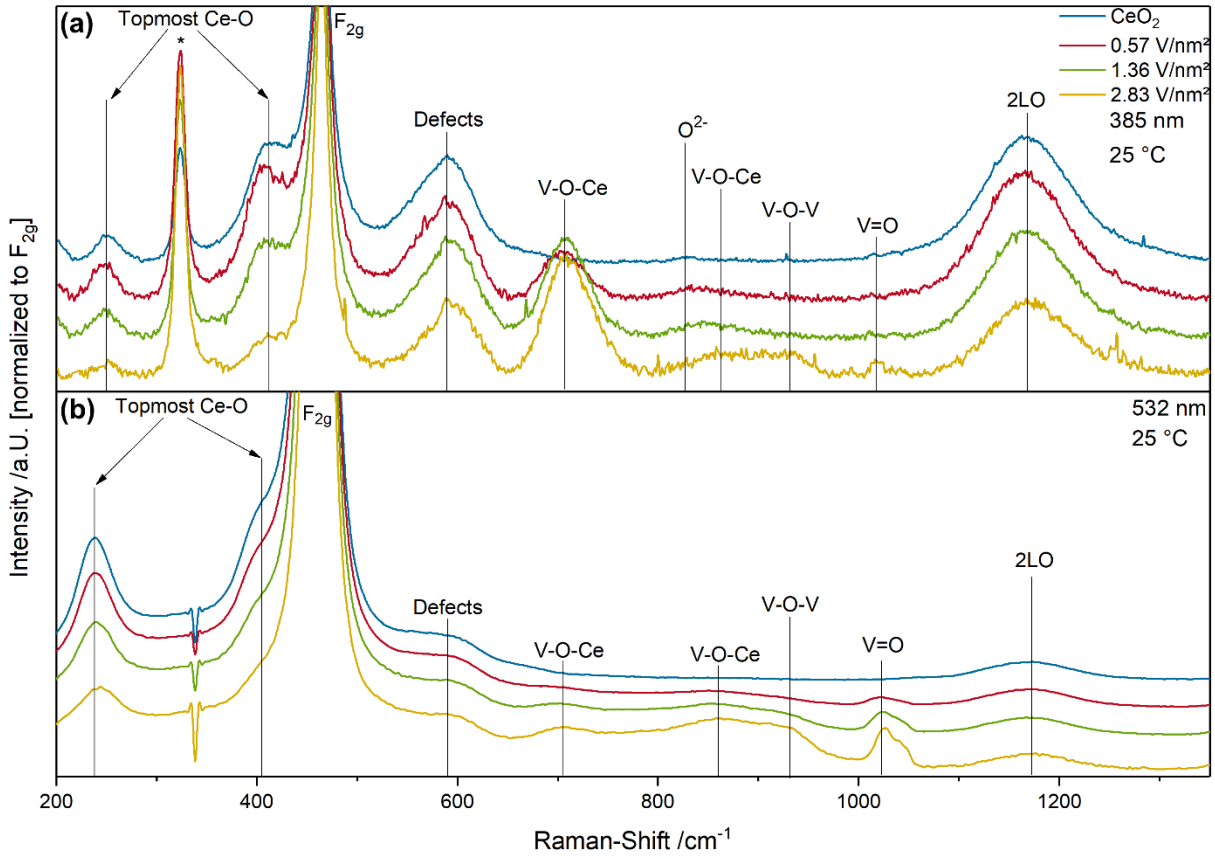

Figure 2: Raman spectra of VO_x/CeO_2 catalysts and bare CeO_2 at 385 nm (a) and 532 nm (b) excitation, recorded at 25 °C after dehydration at 366 °C in 12.5% O_2/He (40 mL_n/min). Spectra are normalized to the F_{2g} peak. The signal of the CaF_2 window is marked with an asterisk. Spectra are offset for clarity.

Furthermore, characteristic ceria bulk features due to F_{2g} (463 cm^{-1}), 2LO (1170 cm^{-1}), and a broad defect peak with a maximum at ~590 cm^{-1} are detected. The latter contains contributions from oxygen vacancies (550 cm^{-1}) and reduced ceria ions (Ce^{3+}, 590 cm^{-1}).[44] With increasing vanadium loading, the position of the F_{2g} peak shows a small shift towards lower wavenumbers (0.3 cm^{-1}). While these changes are very small, they indicate the reduction of ceria when trying to keep vanadium in oxidation state 5+, as has been observed previously for the VO_x/CeO_2 system [16,17,27,28] and described by DFT calculations.[19,22–24,36] Previously observed peroxide peaks at ~830 cm^{-1} are almost absent, due to the oxidative pre-treatment of the catalyst in 12.5% O_2/He at 366 °C for 1 h and subsequent cooling in pure helium.[54]

Vanadia-related features include V-O-Ce interface vibrations at 709 and 860 cm^{-1} and a feature at 930 cm^{-1}, which is still being discussed in the literature[34] but might be assigned to either a V-O-Ce or a V-O-V vibration of dimeric/oligomeric species by comparison with the spectra of vanadates.[28,34,35,55] This is supported by the fact that this feature is only present for the sample with the highest vanadium loading (at 385 nm excitation). Note that at this wavelength, the V=O (vanadyl) stretching vibration at 1023 cm^{-1} is barely visible for samples with low vanadium loading.[35]

Raman spectra recorded at 532 nm excitation show in principle the same features as those at 385 nm excitation (see bottom panel of Figure 2). However, vast differences in the ceria-related peak intensities are observed, owing to the lack of ceria resonance enhancement at 532 nm excitation. The intensity of the V-O-Ce interface peak at 709 cm^{-1} also decreases significantly upon switching from 385 nm to 532 nm, suggesting that this feature might also be resonantly enhanced (also supported by the presence of a small peak at ~1400 cm^{-1}, consistent with the first V-O-Ce overtone), for example by excitation of monomeric/dimeric vanadia species showing UV-Vis absorption below 400 nm. On the other hand, the V-O-Ce and V-O-Ce/V-O-V vibrations at 860 cm^{-1} and 930 cm^{-1} , respectively, become more visible at 532 nm excitation, due to their higher absorption at this wavelength, and increase with vanadium loading, indicating that these features might be assigned to dimeric/oligomeric vanadia.[52] The vanadyl vibration is now clearly visible at all vanadium loadings and shows loading-dependent changes in the profile. In fact, a detailed analysis of the 532 nm spectra (for details refer to the Experimental Section) reveals the presence of (at least) three contributions due to monomeric (~1010 cm^{-1}), dimeric (~1015 cm^{-1}), and oligomeric (>1020 cm^{-1}) species, leading to a broad band in the V=O region.[56] The presence of oligomeric species as indicated by the 532 nm Raman spectra is further confirmed by the band gap energies of the samples (see Tauc plots in Figure S1[44]), which were determined to be 2.88, 2.84, and 2.72 eV, corresponding to 2.9, 3.05 and 3.55 V-O-V bonds for loadings of 0.57, 1.36 and 2.83 V/nm^2, respectively.[52] Table 1 summarizes the detected Raman signals for the VO_x/CeO_2 catalysts together with their assignments.

Table 1: Summary of Raman signals in VO_x/CeO_2 catalysts detected at 385 nm / 532 nm excitation together with their assignments.

Position /cm^{-1}	Assignment	Reference
250	Longitudinal Ce-O surface phonon (contribution from 2TA)	32
405	Transversal Ce-O surface phonon	32
464	F_{2g}	27
590	Defect peak (contributions from $V_O^{\cdot\cdot}$ and Ce^{3+})	27
709	V-O-Ce	26
860	V-O-Ce	26
930	V-O-Ce / V-O-V (?)	26
1010	V=O monomer	26
1015	V=O dimer	26
>1025	V=O in different oligomers	26
1170	2LO	27

Catalytic Measurements. Figure 3 shows the results of the catalytic measurements performed for the VO_x/CeO_2 catalysts and bare CeO_2 during propane ODH (feed: 12.5% O_2/12.5% C_3H_8/He) at a flow rate of 40 mL_n/min between 47 °C and 366 °C. The empty reactor shows no activity up to 320 °C, where it starts to show conversions of < 1% with corresponding propylene selectivities of < 5% at 366 °C. In contrast, bare ceria shows catalytic activity with conversions of up to 20%, but with a maximum propylene selectivity of 5.7 % at 320 °C. Besides propylene and some CO, mainly CO_2 is produced over bare ceria, indicating high activity for total oxidation of propane, as described in the literature.[9,25,57] A similar behavior was observed for ODH reactions with other alkanes e.g. ethane [16,17,27]. In comparison, upon vanadium deposition, the conversion first significantly decreases for the VO_x/CeO_2 sample with 0.57 V/nm² loading and then shows a near-linear decrease with further vanadium loadings (e.g. at 275 °C). This behavior differs from other ODH reactions, for example, the ODH of ethanol.[5] On the other hand, the selectivity of the catalyst increases significantly with vanadium loading, as was reported previously for highly dispersed vanadia on different supports and under different reaction conditions. [7,16,17,27,58,59] Selectivities for

conversions > 1 % reach up to 46 % for 2.83 V/nm² at 275 °C, which is 17 times the increase compared to bare ceria, emphasizing the dramatic selectivity increase when ceria is loaded with vanadium. On the whole, the observed conversions and selectivities are of the same order of magnitude as those previously reported in the literature,[9,25,57] however, the absolute values are influenced by different aspects, such as reactor geometry, the catalyst mass, and retention time.

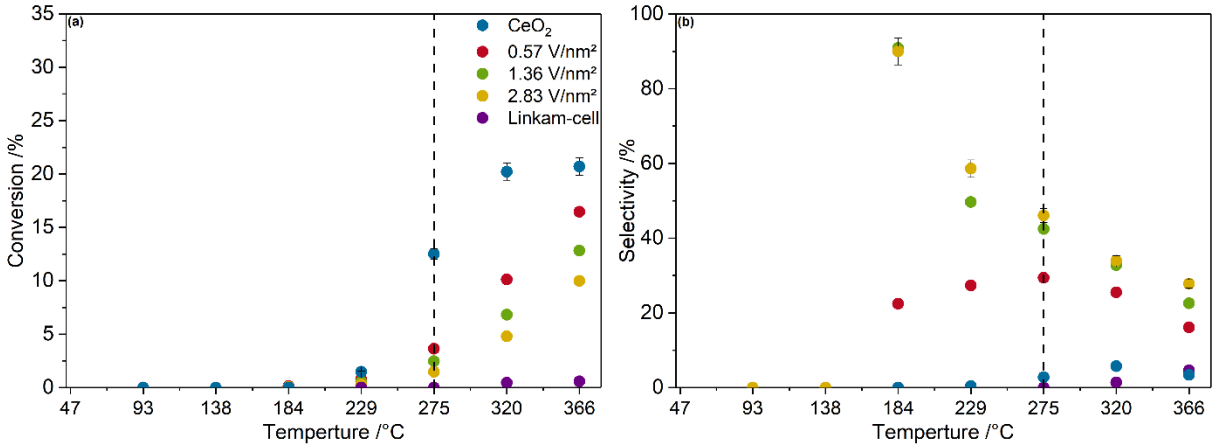

Figure 3: Temperature-dependent propane conversion (a) and propylene selectivity (b) of the VO_x/CeO2 catalysts and bare CeO_2 during propane ODH at a flow rate of 40 mLn/min (feed: 12.5% O_2/12.5% C_3H_8/He). The surface temperature of the sample is given on the bottom axis. The temperature chosen for the *operando* measurements is indicated by the dotted line. Error bars have been added exemplarily for bare ceria (conversion) and the VO_x/CeO_2 sample with 2.83 V/nm², those of the other samples are of the same order of magnitude.

The above results indicate that the presence of vanadia decreases the total oxidation potential and the reaction rate, leading to smaller conversions and higher selectivities. This increase in selectivity cannot be caused just by a decrease in conversion, since the selectivities of the 1.36 and 2.83 V/nm² samples at 320 °C are almost equal, whereas the observed conversions differ by ~3%. Therefore, further effects need to be considered to explain the observed catalytic behavior in addition to the dependence between conversion and selectivity.

For the *operando* experiments presented in this work, a reaction temperature of 275 °C was chosen. At this temperature, a contribution of homogeneous gas-phase reactions

can be excluded. Besides, conversions range between 1.5 % and 12.5 % (differential conditions), with corresponding propylene selectivities between 46 % and 2.8 %, allowing relations between structure and activity to be captured. In the following, *operando* spectroscopy is applied to gain mechanistic insight into the structural dynamics of the catalyst under reaction conditions.

Raman Results. The left side of Figure 4 depicts Raman spectra at 385 nm excitation for bare ceria (top panel) and the VO_x/CeO_2 catalyst with a loading of 1.36 V/nm² (bottom panel), both under oxidizing and under reaction conditions (*operando*) at 275 °C. Corresponding spectra recorded for the other catalysts (0.57 and 2.83 V/nm²) are shown in Figure S2. In the following, we will focus on the transversal Ce-O surface phonon and the defect area (385 nm spectra), on the vanadyl feature (514 nm spectra), and on the F_{2g} peak (532 nm spectra). Spectra were normalized to the F_{2g} peak. The insets show the shifts of the F_{2g} peaks upon switching from oxidative to reactive conditions, recorded at 532 nm excitation. The right side of Figure 4 shows the corresponding gas-phase compositions as analyzed by GC, as well as the conversions and selectivities for each sample.

Upon switching from oxidizing to reaction conditions, multiple changes are observable in the recorded spectra. For bare ceria, there is a significant reduction in intensity of the transversal topmost Ce-O surface vibrations, which is indicative of reduction of the ceria surface owing to hydroxyl group formation by hydrogen abstraction from propane and subsequent formation of water, resulting in oxygen defect formation (see Figure 11). This step may also follow a hydrogen abstraction from propane to the vanadia species and a fast hydrogen transfer to the ceria surface, so that a change in Raman intensity cannot be observed. However, this does not change the overall mechanism described in this study, since either way hydrogen is finally transferred to the ceria surface (see Figures 8 and 9). The intensity change decreases with increasing vanadium loading (compare Figure 5), which correlates with the decline in conversion with increase in vanadium loading, further supporting the idea that the reduction in Ce-O intensity originates from propane ODH.

The redshift of the F_{2g} peak (see inset) implies a reduction of the ceria subsurface due to lattice expansion upon oxygen vacancy formation, as previously described in the literature.[51] To work out this effect more clearly, we employed 532 nm laser excitation with its deeper penetration depth compared to 385 nm excitation. Subsurface reduction may be caused by diffusion of surface defects into subsurface layers. As a consequence, diffusion of

subsurface oxygen to the catalyst surface is expected, representing a source of ceria surface regeneration besides gas-phase oxygen. The extent of the F_{2g} redshift (see Figure 5c) also correlates with the observed conversion changes with increasing vanadium loading, whereas vanadia does not seem to be taking an active part in the reaction since we do not observe any changes in the Raman intensity of vanadia-related features upon switching from oxidizing to reaction conditions.

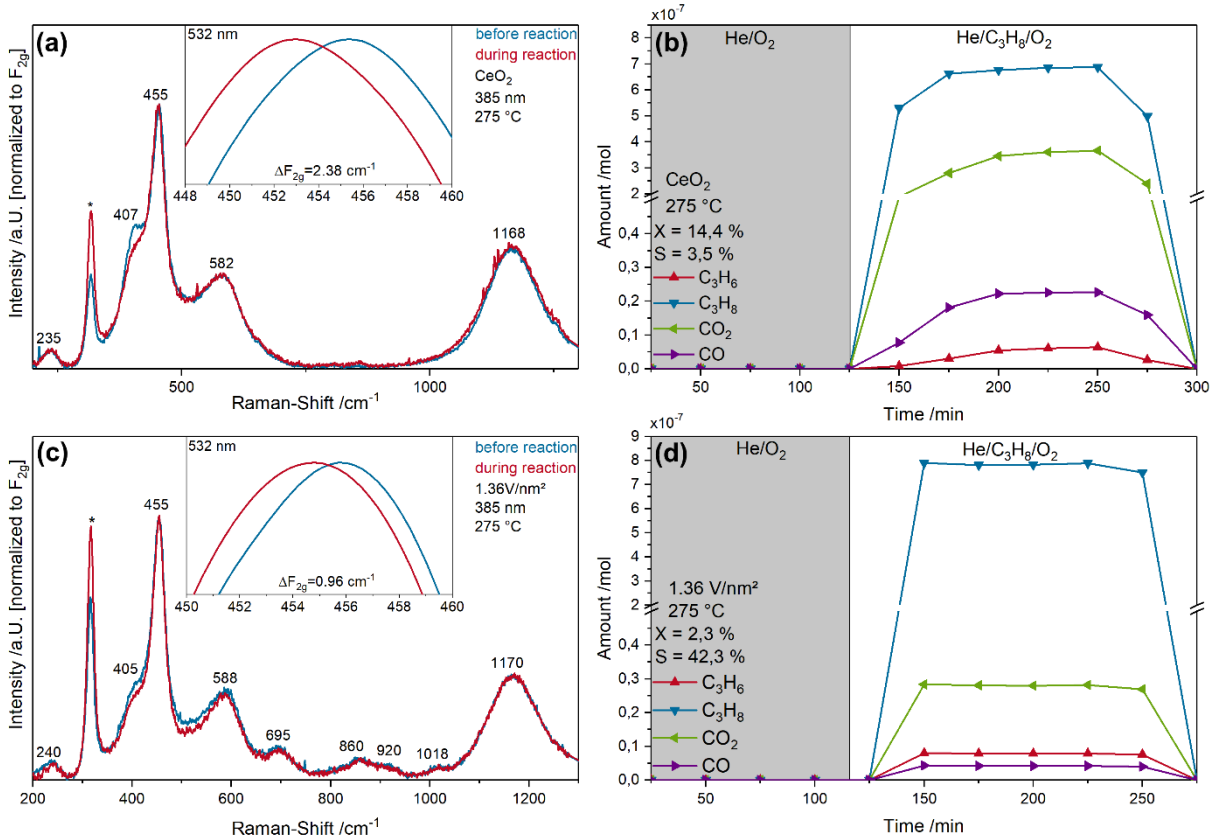

Figure 4: *Operando* 385 nm Raman spectra (red) of bare ceria (a) and VO_x/CeO_2 (1.36 V/nm²) (c) at 275 °C, compared to spectra recorded prior to reaction under oxidative conditions (blue). Spectra have been normalized to the F_{2g} peak. The signal from the CaF_2 window is marked with an asterisk. The insets give enlarged views of the F_{2g} maxima recorded at 532 nm excitation. The corresponding gas-phase compositions under oxidizing and reactive conditions are shown on the right for bare ceria (b) and VO_x/CeO_2 (1.36 V/nm²) (d) together with the propane conversions and propylene selectivities. Note that the y axis is interrupted between 0.5 and 2 mol for clarity.

Besides the dynamics of the surface phonon mode and the F_{2g} peak, we observe significant intensity changes in the defect area (500-650 cm^{-1}) of the VO_x/CeO_2 samples, which are not detected for bare ceria. This difference in behavior is attributed to the ability of ceria to act as an oxygen ion conductor, regenerating surface oxygen vacancies fast enough for changes in the surface oxygen defect concentration not to be observed. In contrast, for ceria loaded with vanadium, the defect band decreases under reaction conditions. Since the oxygen dynamics in the ceria lattice is reduced upon vanadium loading (see F_{2g} shift in Figure 5c), the surface oxygen defect concentration may be expected to show an increase. This apparent discrepancy might be explained by interactions between vanadia and ceria oxygen defects proposed by Wu et al.[34,35] and further supported by DFT calculations by Penschke et al. showing a structural relaxation of vanadia monomers into ceria surface oxygen defects, thereby blocking defect sites[22] and decreasing their concentration. The defect band region was investigated in more detail by Schilling et al.,[53] who conclude that oxygen-vacancy-containing contributions to the overall defect band occur in the same spectral region as the dynamics observed in the Raman spectra (see Figure 4), which provides additional support for the hypothesis that the observed decrease is caused by surface vanadia after structural relaxation into the vacancy. Since the diffusion barrier of vanadia species on a ceria surface is not overcome at this temperature,[23] the sites are irreversibly blocked. As can be seen on the right side of Figure 4, propane ODH over VO_x/CeO_2 catalysts does not lead to an increase in the amount of propylene but rather to a significantly reduced CO_2 production; based on the above findings, we propose the interaction between vanadia and oxygen vacancies to be responsible for the slowdown in oxygen dynamics during propane ODH resulting in a decreasing CO_2 production.

Figure 5 depicts the changes in Raman intensity of the transversal Ce-O surface phonon (a) and the defect band (b) for VO_x/CeO_2 samples and bare ceria, based on the 385 nm Raman spectra shown in Figure 4. Dashed lines represent spectra recorded under oxidizing conditions and solid lines those recorded under reaction conditions. Spectra are offset for clarity. To quantify the observed changes, we calculated difference spectra and integrated the resulting areas (see Figure 5c). Figure 5c also contains F_{2g} shifts, which were determined by fitting Lorentzian curves to the F_{2g} peaks under oxidizing and reaction conditions.

Figure 5a shows that the intensity changes of the transversal Ce-O surface phonon upon switching from oxidizing to reaction conditions decline with increasing vanadium

loading. As can be seen in Figure 5b, changes of the defect band intensity first increase from bare ceria to low-loaded VO_x/CeO_2 (0.57 V/nm²), but then decrease almost linearly with a further increase in vanadium loading. This behavior indicates that not all surface vanadia species are capable of interacting with oxygen vacancies but rather only those present at low loadings. According to the DFT study by Penschke et al.,[22] monomeric vanadia species are able to relax in to nearby oxygen defect sites. This was also verified by *operando* XANES [27] and, further supporting the hypothesis of monomeric vanadia species interacting with ceria active sites. Conversely, this means that defect sites further away from monomeric vanadia species should be able to be regenerated by oxygen. The F_{2g} mode also shows a smaller redshift with increasing vanadia loading, indicating less reduced ceria states in the subsurface. This trend correlates with the observed conversion and indicates that ceria reduction is an important feature during the redox cycle of propane ODH. Furthermore, due to blocking of defect sites by vanadia, the defects are not able to diffuse into the subsurface of the catalyst but rather stay at the surface, thus further decreasing the observed F_{2g} shift. This is also shown by the trend of the defect peak difference area where the area differences are large and in a similar order of magnitude for 0.57 and 1.36 V/nm², which leads to a reduced F_{2g} redshift in comparison to bare ceria. The area difference of the defect peak of the 2.83 V/nm² catalyst is comparable to that of the bare ceria. Therefore, the very small F_{2g} redshift is likely to be influenced mainly by the significantly reduced conversion (see DRIFTS section for an explanation of the reduced conversion at 2.83 V/nm²).

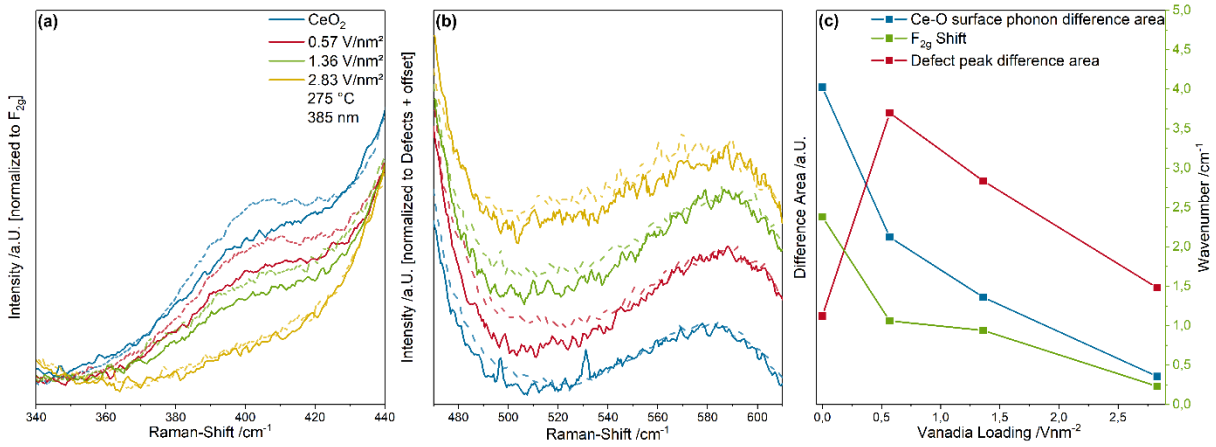

Figure 5: Raman intensity change of (a) the transversal surface phonon and (b) the ceria defect region (normalized to the defect peak at 590 cm^{-1}) with increasing vanadium loading based on the 385 nm spectra shown in Figure 4. Dashed lines represent the spectra recorded under

oxidizing conditions and solid lines those recorded under reaction conditions. Spectra are offset for clarity. The intensity changes are summarized in (c) together with the F_{2g} shift plotted as a function of vanadium loading.

As a basis for a more detailed structural analysis of the vanadia species present on the ceria surface, Raman spectra were recorded under oxidizing conditions at 275 °C at 514 nm excitation to enhance the vanadia signals (especially the V=O stretching signal) compared to 385 nm excitation. The nuclearity of the vanadia species can be determined from the different frequency positions of the vanadyl peak, as discussed previously in the literature.[56] The full Raman 514 nm spectra (see Figure S3) do not provide any further mechanistic insight in comparison to those recorded at 385 nm excitation. Hence, the following discussion focuses on the vanadyl stretching region, which is shown in Figure 6 together with characteristic V=O stretching frequencies of vanadia species with different nuclearities. Slight variations in the V=O positions at different nuclearities are expected due to the influence of dipole interactions of neighboring V=O groups. The V=O stretching contribution with the lowest wavenumber is found to be located at 1008 cm^{-1}, in good agreement with the literature, attributed to a monomeric vanadia species.[35],[36] Further blueshifted features were then assigned to vanadia species with one more V-O-V bond each. Accordingly, the five contributions at 1008, 1016, 1023, 1030, and 1040 cm^{-1} are assigned to monomeric, dimeric, trimeric, tetrameric, and heptameric species, respectively. These positions are similar to those reported previously in the context of Raman and IR spectra.[35],[36] Please note that Raman spectra recorded at 532 nm and 25 °C gave a slightly higher value for the monomeric species (see Table 1) than that detected at 514 nm and 275 °C (see Figure 6), consistent with thermal effects.

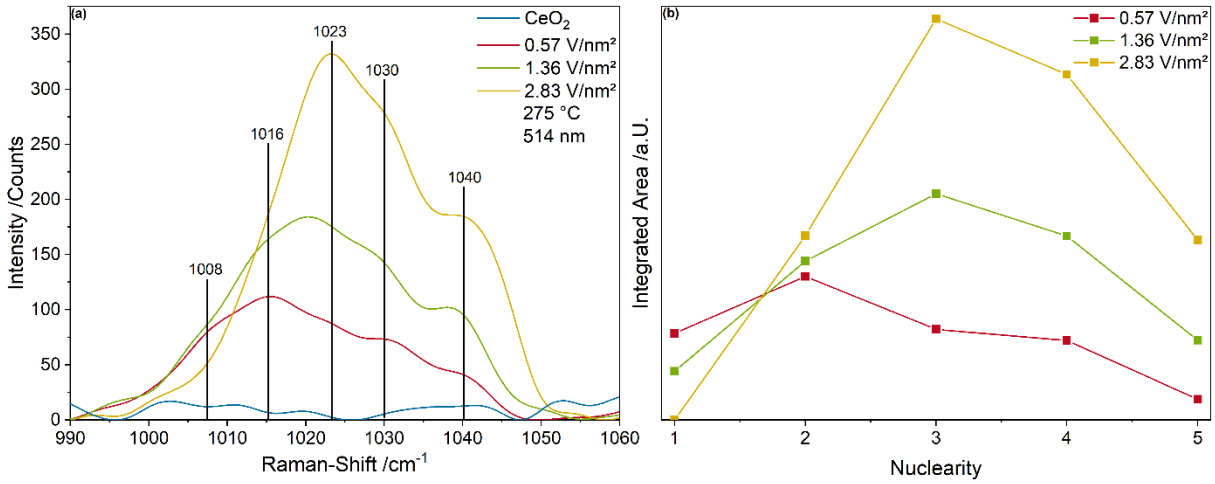

Figure 6: Vanadyl stretching region of 514 nm Raman spectra (a) recorded under oxidizing conditions at 275 °C for VO_x/CeO_2 and bare ceria. Marked V=O stretching frequencies indicate vanadia species of different nuclearity. From a peak fitting analysis (compare Figure S4) the areas shown in (b) are obtained.

To quantify the fraction of each surface vanadia species, the vanadyl signal was fitted using five Lorentzian functions, as shown exemplarily in Figure S4 for a loading of 0.57 V/nm². Figure 6b summarizes the resulting areas as a function of nuclearity. For the lowest vanadium loading (0.57 V/nm²), dimers are found to be the most common vanadia species on the ceria surface, whereas trimers are most common for higher loadings. According to theoretical calculations, trimeric species are predicted to be the most stable species on a ceria (111) surface.[22] As discussed before, the observed changes in the defect band intensities (see Figure 5) may be attributed to the interaction with surface vanadia, most likely monomeric species. In fact, the concentration of monomeric species decreases linearly with the vanadium loading and therefore correlates with the trend observed for the defect intensity changes, whereas the concentration of all other species increases with the vanadium loading. Furthermore, for the sample with a loading of 2.83 V/nm², almost no intensity changes in the defect region as well as no monomeric species in the 514 and 532 nm Raman spectra are observed. This behavior is in good agreement with DFT results predicting vanadia monomers to engage in interactions with defects, as mentioned above in the context of Figure 5.[22]

DR UV-Vis Results. The application of *operando* UV-Vis spectroscopy may provide additional information about the structure of ceria-supported vanadia, but it also allows us to ensure

that the dynamics observed in the Raman spectra do not result from changes in sample absorption during reaction, thereby changing the extent of resonance enhancement. Figure 7 depicts *operando* UV-Vis spectra of bare ceria (a) and VO_x/CeO_2 (1.36 V/nm²) (b) at 275 °C, compared to spectra recorded under oxidative conditions prior to reaction. The corresponding spectra for the other loadings (0.57 and 2.83 V/nm²) are shown in Figure S5. The laser excitation wavelengths (385, 514 and 532 nm) used in this study are indicated, showing no significant changes in absorption between the two conditions. Band gap shifts between spectra measured under oxidizing and reaction conditions were determined using Tauc plots, and the d-d transition intensity caused by reduced vanadium states[60,61] was determined by comparing intensities at 700 nm. Figure 7c summarizes these results as a function of vanadium loading.

As can be seen from Figure 7, the absorption changes caused by the exposure to reaction conditions are very small at the excitation wavelengths chosen for Raman spectroscopy. Furthermore, for resonantly enhanced spectra, a change in the ceria, vanadia, or a combination of ceria and vanadia absorption behavior would not be expected to affect only one Raman feature (e.g. the transversal Ce-O surface phonon) but rather multiple features. Based on the *operando* UV-Vis data we therefore conclude that the dynamics in the Raman spectra originates from switching the gas environment from oxidative to reactive rather than changes in the absorption behavior at the excitation wavelengths.

More detailed analysis of the UV-Vis spectra using Tauc plots[44] reveals small but reproducible changes in the band gap energy. The band gap shifts by 0.05 eV between oxidizing and reaction conditions for bare ceria but shows even smaller shifts for the VO_x/CeO_2 samples, i.e., 0.01eV for the 1.36 V/nm² sample. Note that the values determined for the samples loaded with 1.36 V/nm² and 2.83 V/nm² are within the margin of error. However, the general trend of the band gap shifts indicates the reduction of ceria during propane ODH and the observed band gap shifts also correlate with the conversion observed with increasing vanadium loading. The correlation between the degree of reduction and the band gap has already been proposed by Flitschew et al.[44] based on UV-Vis and Raman spectra at 514 nm excitation and is supported by a first principles DFT study by Skorodumova et al.,[62] suggesting that Ce(III) oxide has a smaller band gap than Ce(IV) oxide. This observed band gap shift also correlates with the observed F_{2g} shift from Raman results, indicating that the results from the different methods are consistent. This shows quite clearly, that the bare ceria is

reduced most during reaction conditions, whereas an increasing vanadia loading leads to less and less ceria reduction. This is similar to results obtained during ethane ODH. [17]

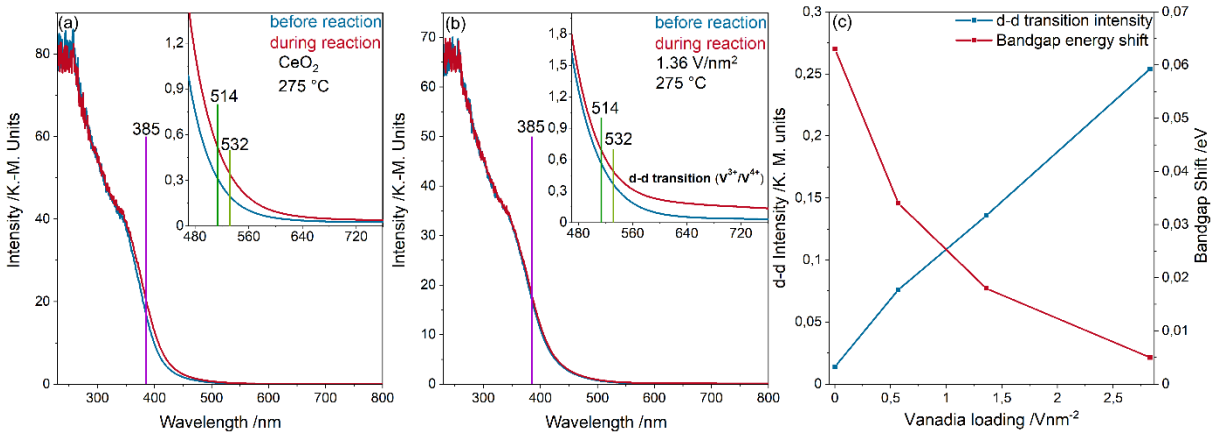

Figure 7: *Operando* UV-Vis spectra (red) of bare ceria (a) and VO_x/CeO_2 (1.36 V/nm²) (b) at 275 °C, compared to spectra recorded under oxidative conditions prior to reaction (blue). The laser excitation wavelengths (385, 514, and 532 nm) are indicated. Insets highlight the region between 470 nm and 760 nm. Band gap shifts were determined using Tauc plots and the d-d transition intensity was determined based on intensities measured at 700 nm (c).

As indicated in the insets of Figure 7, upon switching from oxidative to reactive conditions, an increase in absorption at higher wavelengths is observed, which originates from d-d transitions of reduced vanadia species (e.g. V^{3+}/V^{4+}),[60,61] and which increases with the vanadium loading. Nevertheless, the relative d-d transition intensities are significantly smaller than those observed for catalyst systems in which vanadia takes part in the reaction or is reduced.[63,64] Therefore, vanadia is either reduced to a very small extent or most of the vanadia is regenerated very fast by ceria to vanadium (V), which would be consistent with previous experimental [16,17,35] and theoretical work [23,37,65]. The observed d-d intensity increases with vanadium loading (see Figure 7c) but does not correlate with the observed conversion, indicating that the presence of reduced vanadia species is not linked to the ODH of propane but is rather caused by other effects, such as a generally increased reducibility of the catalyst or a very fast hydrogen transfer from the vanadia to the ceria surface and a very slow further conversion on the ceria surface due to blocked defect sites. This is supported by the fact that there are no observable intensity changes for any vanadia-related features in the Raman spectra on switching to reaction conditions. The small changes in d-d transition

intensity and the absence of intensity changes for vanadia related features in 385 nm Raman spectra indicate that vanadia remains largely unchanged during propane ODH or is regenerated very fast after the first C-H hydrogen abstraction to the catalyst surface.

The changes in band gap energy observed in the UV-Vis spectra are indicative of a reduction of the ceria (sub)surface during the reaction. This behavior is fully consistent with the 385 and 532 nm Raman results described above (see Figure 5c). In fact, the reduction of the ceria surface is indicated by the Ce-O intensity decrease in the 385 nm Raman spectra, whereas the ceria subsurface reduction is evidenced by the F_{2g} redshift at 532 nm excitation.

DRIFTS Results. Based on the results from operando Raman and UV-Vis spectroscopy we propose the ceria support to be actively taking part in the ODH of propane. As discussed for the catalytic measurements, a decrease in conversion cannot be the only reason for the increase in selectivity with increasing vanadium loading, since VO_x/CeO_2 samples with different loadings at the same conversion had different selectivities. The observed decrease in conversion and increase in selectivity of the 0.57 V/nm² catalyst (compared to bare ceria) could be rationalized by an interaction between monomeric vanadia species and ceria oxygen defect sites, which is consistent with previous experimental results [16,17,27,28,35] also showing that dispersed vanadia interacted with ceria active sites. However, this effect cannot explain the further selectivity increase when more vanadia is added, since the concentration of monomeric species was shown to decrease at higher vanadium loadings. Therefore, a decrease in selectivity would be expected for higher vanadium loading despite the decrease in conversion. Since this is not detected, other effects not accessible by Raman and UV-Vis may be responsible for the observed behavior. To gain additional insight, particularly regarding the presence of adsorbates and their role in propane ODH, *operando* DRIFT spectra were measured.

Figure 8 presents DRIFT spectra of bare ceria (a) and VO_x/CeO_2 loaded with 1.36 V/nm² (b) during oxidizing and reaction conditions. Since the formation of hydroxyl groups via hydrogen transfer from propane to the ceria surface has been conjectured as a possible reaction step (see above), isotope experiments using propane-d_8 were performed to verify the formation of Ce-O-D groups. The corresponding spectra for the other VO_x/CeO_2 samples (0.57 and 2.83 V/nm²) can be found in Figure S7. For details of the data processing please refer to the Experimental Section; as an example, the processing steps are illustrated in Figure S6 for the VO_x/CeO_2 sample with 1.36 V/nm² loading.

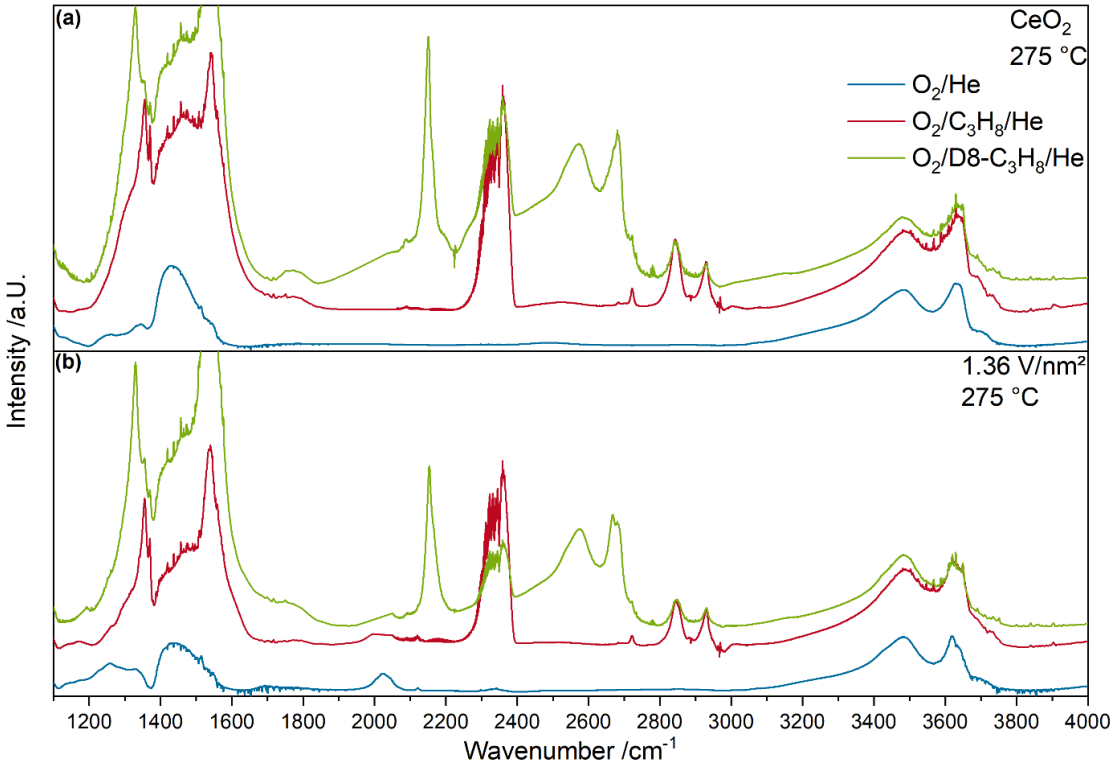

Figure 8: DRIFT spectra of bare ceria (a) and VO_x/CeO_2 (1.36 V/nm²) (b), recorded under oxidizing conditions, reaction conditions, and reaction conditions with propane-d_8 at 275 °C.

According to Figure 8, spectral changes upon switching from oxidizing to reaction conditions are mainly detected within the ranges 1200-1800 cm^{-1} and 2700-3000 cm^{-1}. Furthermore, there is an overall intensity increase in the O-H stretching region (3400-3750 cm^{-1}), as well as new features at 3690 cm^{-1} and at 3734 cm^{-1} due to Ce-O-H groups.[66] These will be discussed in more detail below in the context of Figures 9 and 10. Additional peaks are observed at ~2050 cm^{-1} and within 2250-2400 cm^{-1}, which may originate from the first overtone of the V=O stretching vibration[67] and gas-phase CO_2 produced by the reaction, respectively. When propane-d_8 is used instead of regular propane, new signals appear in the range 2500-2750 cm^{-1} with the same profile as that of the O-H stretching bands, evidencing the presence of O-D stretching vibrations. The peaks at 2720 cm^{-1} and at 2770 cm^{-1} are assigned to be a Ce-O-D vibration since the CH_2 vibration from propane at this position should not be present with a significant intensity for propane-d_8, confirming the abstraction of hydrogen from propane to the ceria surface. Furthermore, the position of the Ce-O-D features at 2720 cm^{-1} and 2770 cm^{-1} is in good agreement with those expected for the Ce-O-H vibrations at 3690 cm^{-1} and 3734 cm^{-1}, when hydrogen is replaced by deuterium. In addition,

a peak at ~2150 cm^{-1} is detected. This peak is assigned to a CDH vibration of gas-phase propane-2-d_1, in agreement with the literature,[68] formed over the ceria surface via isotope scrambling between regular propane and propane-d_8. In the DRIFT spectra in Figure 8, this peak is the only detected gas-phase signal, since gas-phase contributions from propane and propane-d_8 have been subtracted and there is no indication of H/D exchange of the CH_3/CD_3 group. For the VO_x/CeO_2 samples, there are no apparent changes in the nature of the adsorbates observed, neither for regular propane nor for propane-d_8. Therefore, we conclude that the observed adsorbates are essentially the same for ceria and VO_x/CeO_2 samples.

For a more detailed analysis, Figure 9 gives an enlarged view of the regions 1200-1800 cm^{-1} (a; carbonate), 2650-3000 cm^{-1} (b; carbohydrates), and 3400-3750 cm^{-1} (c; O-H stretching). Dashed lines represent the respective under oxidizing conditions, while solid lines represent *operando* spectra after subtraction of the spectra obtained under oxidizing conditions. Spectra are offset for clarity. The assignments for the features in Figure 9 are summarized in Table 2. The peaks at 2686 cm^{-1} and 2722 cm^{-1} are assigned to C-H stretching vibrations of propane adsorbed to the ceria surface (possibly C_3H_7 species) in different configurations. Note that the latter assignment follows a previous study on Pd/CeO_2,[39] which did not report the 2686 cm^{-1} peak, probably for sensitivity reasons.

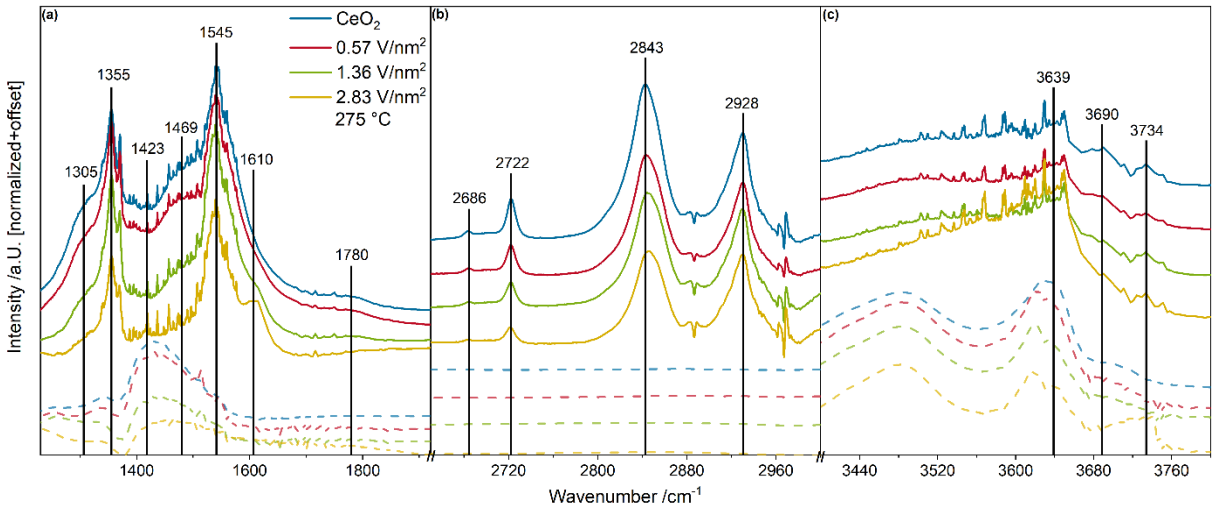

Figure 9: Enlarged view of the carbonate (a), the carbohydrate (b) and the O-H stretching (c)[65,66,69–72] regions based on the DRIFT spectra shown in Figure 8. Dashed lines represent spectra under oxidizing conditions and solid lines represent *operando* spectra after subtraction of the spectra under oxidizing conditions. Spectra are offset for clarity.

Table 2: Assignments of IR features detected for VO_x/CeO_2 catalysts and bare ceria during propane ODH at 275 °C.

Position /cm^{-1}	Assignment	Reference
1305	υ_s C-O	18
1355	υ_s CH_3	18
1423	υ_s COO	18
1469	δ_{as} CH_3	18
1545	υ_{as} COO	18
1610	υ_{as} O-C-O	58
1780	υ C-O	62
2686	υ C-H (?)	this work
2722	υ C-H	35
2843	υ CH_2	18
2928	υ CH_2	18
3639	Ce-O-H II-B	57
3690	Ce-O-H II*-A	57
3734	Ce-O-H I-A	57

The Ce-O-H stretching region shows changes in intensity between oxidizing and reaction conditions (see Figure 9c). Three distinct types of hydroxyl groups are identified in the difference spectra at 3639, 3690, and 3734 cm^{-1}, which have previously been attributed to II-B, II*-A, and I-A Ce-O-H vibrations, respectively.[66] Type I represent mono-coordinated, and type II doubly bridging hydroxyl groups. According to the literature, a II-B hydroxyl corresponds to a doubly bridging hydroxyl group adjacent to a surface oxygen vacancy, whereas a II*-A hydroxyl results from a doubly bridging hydroxyl group with cerium reduction.[57] For the hydroxyl group at 3639 cm^{-1} no equivalent Ce-OD feature was observeable since it overlaps heavily with the D_2O region. Since D8-propane was only present during the reaction conditions, no difference spectra are available. The observation of these hydroxyl features further supports the hypothesis that hydrogen is first abstracted from propane and then transferred to the ceria surface (either by ceria directly or via vanadia structures with a

subsequent fast transfer to the ceria surface), forming hydroxyl groups. While Figure 9 shows that the nature of the adsorbates does not change with increasing vanadium loading, a change in their relative concentrations can be detected. The most common adsorbates, according to Figure 9, are carbonates characterized by signals at 1305, 1423, 1545, and 1780 cm^{-1}.[20,65,69,71,73] In addition, C-H stretching vibrations of CH_2 groups in propane adsorbed to ceria are observed at 2928 and 2843 cm^{-1}.[20] In the following, the peaks within the range 1300-1800 cm^{-1} will be related to oxygen-containing adsorbates due to their high oxygen content, whereas the peaks between 2680 and 2930 cm^{-1} will be related to oxygen-free adsorbates.

The adsorbate features in Figures 9a and b show changes in intensity with increasing vanadium loading, particularly, those of the oxygen-containing adsorbates, but no completely new features. One exception is the peak at 1610 cm^{-1}, previously assigned to carbonates,[71] which first appears for the sample loaded with 0.57 V/nm² and then increases in intensity for higher vanadium loadings. There is no indication of this peak on bare ceria, which may be explained by its higher oxygen dynamics facilitating the oxidation of carbonates to CO_2. With increasing vanadium loading, the oxygen dynamics are slowed down (see above); thus carbonates might stay (longer) on the surface, possibly blocking reaction sites.

To quantify the changes in adsorbate intensity, the selected regions from Figures 9a and b were fit using Lorentzian functions. As an example, this is illustrated in Figure S8 for VO_x/CeO_2 loaded with 0.57 V/nm². Figure 10 depicts the resulting peak areas of selected adsorbate peaks for (a) oxygen-free adsorbates (represented by the symmetric and asymmetric CH_2 stretching vibrations at 2843 and 2928 cm^{-1}) and (b) oxygen-containing adsorbates (represented by the asymmetric COO stretching vibration at 1545 cm^{-1}, the symmetric COO stretching vibration at 1423 cm^{-1}, and the symmetric C-O stretching vibration at 1305 cm^{-1}) as a function of vanadium loading.

As can be seen in Figure 10, the peaks related to the oxygen-containing adsorbates show a more pronounced intensity decrease with increasing vanadium loading than those related to the oxygen-free adsorbates. In fact, a sharp drop is observed for an increase in vanadium loading from 0.57 V/nm² to 1.36 V/nm², which may indicate a weaker adsorption of propane, probably caused by changes in the vanadia surface structure. The weaker adsorption may facilitate the transformation of a higher proportion of propane to propylene and its

desorption from the catalyst surface before it is fully oxidized to CO_2, thereby decreasing the detectable presence of oxygen-containing adsorbates and increasing the overall selectivity.

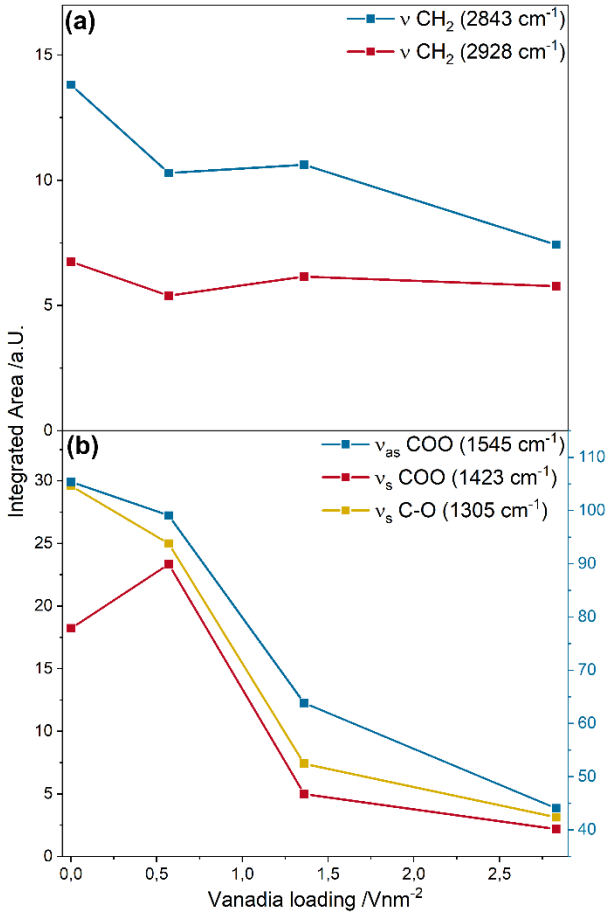

Figure 10: Selected adsorbate features relevant to the discussion of the mechanism of propane ODH. The areas result from a fit analysis to the *operando* DRIFT spectra shown in Figure 9a and b. The features in (a) and (b) are related to oxygen-free and oxygen-containing adsorbates, respectively.

Mechanistic Discussion. In the following, we will discuss the findings from Raman, UV-Vis, and IR spectroscopy presented in the previous sections with regard to their mechanistic insights into the ODH of propane over VO_x/CeO_2 catalysts.

The presence of vanadia monomers, dimers, and oligomers on the catalyst surface was evidenced by their contributions to the vanadyl band in the 514/532 nm Raman spectra. Since all detected vanadyl signals were located above 1000 cm^{-1}, we conclude that the VO_x/CeO_2

catalysts do not contain (micro)crystalline V_2O_5. Furthermore, there is no indication of the presence of $CeVO_4$ in the Raman spectra, in agreement with the literature, as these structures would be expected at higher temperatures and vanadia loadings or more reducing conditions than proapne and oxygen such as pure propane or H_2.[35,57] Thus, in the VO_x/CeO_2 catalysts studied here, vanadia is present exclusively as monomeric, dimeric, and oligomeric surface species.

The first step of the reaction mechanism is the adsorption of propane onto the catalyst surface, which involves the abstraction of a hydrogen atom from propane and its transfer to ceria surface lattice oxygen. This is experimentally confirmed under reaction conditions by the intensity decrease of the transversal Ce-O surface phonon in the UV-Raman spectra and the detection of Ce-O-D stretching vibrations in the propane-D_8 DRIFT spectra. To this end, DFT studies have suggested a hydrogen transfer to surface oxygen located in close proximity to the propane adsorption site.[37] As a result of the first reaction, intermediary $C_3H_7^*$ is formed (see Figure 11), from which a second hydrogen may either be abstracted to the same ceria site as the first hydrogen, leading to Ce-OH_2 formation, or to another surface lattice oxygen atom to yield a second hydroxyl group. Both scenarios result in a decrease of the transversal Ce-O phonon intensity and are therefore consistent with the experimental results (see Figures 4 and 5). As also DFT studies have considered both as likely, based on their very similar energies,[37] it is currently not possible to favor one of the above scenarios.

In the last step, propylene desorbs from the catalyst surface and water is formed from both abstracted hydrogen atoms and one surface lattice oxygen atom, resulting in an oxygen defect site (see Figure 11). The formed surface oxygen defect may then interact with vanadia monomers in close proximity to the defect site, as suggested by the UV-Raman spectra (see Figures 4 and 5). Please note that of all detected surface vanadia species only the monomers follow the same trend as the observed decrease in defect intensity. These findings are supported by DFT results,[22] showing that the monomeric vanadia species hereby undergoes structural relaxation into the formed vacancy, resulting in an irreversible blocking of the vacancy. As a consequence, the overall oxygen dynamics in the catalyst are slowed down, thereby increasing the selectivity. On the other hand, vacancies located further away from vanadia monomers are not influenced by this interaction.[22]

The *operando* DRIFT spectra provide information on the presence of adsorbates on bare ceria and on the VO_x/CeO_2 catalysts under reaction conditions. With increasing vanadium

loading, a continuous decrease in adsorbate intensity but no apparent change in the nature of the adsorbates is observed. On the other hand, the pronounced influence of vanadia on the catalytic performance is expected to influence the propane adsorption/reaction behavior. The detection of higher adsorbate concentrations for bare ceria points to a stronger adsorption compared to VO_x/CeO_2, thus resulting in more total oxidation products such as CO_2 (or CO), for example via formation of different intermediates as proposed previously,[74] while the presence of vanadia may increase the selectivity by decreasing the adsorption strength of propane and reaction intermediates to the surface. This hypothesis is supported by the observation that the peaks related to the oxygen-containing adsorbates strongly decrease with vanadium loading, while those of the oxygen-free features show much smaller variations (see Figure 10). Regarding the adsorption of propane on VO_x/CeO_2 catalysts, one may in principle envisage an adsorption onto ceria influenced by the presence of nearby vanadia or the direct adsorption onto vanadia surface structures.[12,75] As switching from oxidative to reactive conditions did not lead to any changes in the vanadia-related Raman features (see Figure S3), the rate-determining step, which has been proposed to be the first hydrogen abstraction, is proposed to proceed without bond breaking in the vanadia structure (see Figure 11). While our results do not allow for a further specification of the propane adsorption/reaction site, the exclusive involvement of vanadia monomers appears rather unlikely, as the fraction of monomeric species shows a strong decrease with increasing vanadium loading and even disappears for 2.83 V/nm², while the loading-dependent catalyst properties show a different behavior. More detailed information on the interaction between surface vanadia and propane may be accessible by future DRIFTS experiments using other propane isotopes such as $CH_3CD_2CH_3$, as previously reported by Chen et al.[75]

Besides reduction of the topmost ceria surface layer detected via the transversal Ce-O phonon intensity as discussed above, there is evidence for the reduction of the ceria subsurface accessible by the F_{2g} redshift in the *operando* visible Raman spectra (see Figures 4 and 5) during reaction conditions, which is consistent with previous experimental data on the VO_x/CeO_2 system recorded under different conditions [27]. This behavior is fully consistent with the *operando* UV-Vis spectra (see Figure 7), which monitor both surface and subsurface and show a reduction-induced redshift of the observed band gap. In fact, the extent of the intensity decrease/redshift is correlated to the observed conversion, indicating that these effects are linked to the reaction. From these findings, we conclude that surface oxygen

vacancies consumed during propane ODH are replenished by oxygen diffusing from the subsurface to the surface, leading to ceria reduction in the subsurface region. This process is likely to occur in parallel with ceria regeneration by gas-phase oxygen, since the conversion of propane stays constant for 3 h (see Figure 4), which is unlikely if only ceria bulk oxygen were consumed without regeneration by gas-phase oxygen. This is further supported by the fact that the amount of oxygen present in CO_2 formed as a reaction product over 3 h for bare ceria (see Figure 5b) exceeds the amount of oxygen present in the 70 mg catalyst sample. Therefore, gas-phase oxygen seems to be the oxygen source during propane ODH. Since a subsurface reduction of ceria is observed, (see Figures 5c and 7c) the regeneration at the active centers is likely due to oxygen diffusion from the subsurface and the gas-phase oxygen probably regenerates the catalyst at a different position. Therefore, ceria acts as an oxygen buffer for the reaction.

The presence of weak d-d transitions in the *operando* UV-Vis spectra indicates a small degree of vanadium reduction. However, as the d-d transition intensity correlates with the vanadium loading rather than the observed conversion and the overall intensity changes are very small, it is suggested that the observed vanadium reduction is not caused by the reaction but rather by unrelated (thermal) processes.

The proposed reaction mechanism for propane ODH over VO_x/CeO_2 catalysts is summarized in Figure 11. Our findings differ from those reported for the ODH of small alcohols (MeOH, EtOH) over VO_x/ceria catalysts, according to which ceria has been proposed to act as an oxygen buffer, regenerating the vanadia species on the surface. In these reactions, surface vanadia species actively participate in the reaction, in particular, via V-O-Ce interface bonds, as shown by our previous *operando* work,[18] which is in contrast to the passive role of vanadia in propane ODH as elucidated in the present study. The origin of this different behavior can be related to the structure of the substrate molecule. Alcohols form stable surface alkoxy species as an intermediate of the reaction, which are readily accessible by spectroscopy, based on which the rate-determining C-H bond breakage and further reaction to the product occurs. In fact, the presence of alkoxy species modifies the V-O-Ce interface bonds and facilitates the subsequent hydrogen transfer, a scenario which is fully consistent with theory.[36] However, despite the differences in reactivity behavior during alcohol and alkane ODH over VO_x/ceria catalysts, vanadium is not participating as a redox system in these reactions.

For propane ODH over vanadia on other supports (e.g. SiO_2 and Al_2O_3), vanadia-related features such as interface bonds (e.g. V-O-support) or the V=O bond have been proposed to be important for the reaction mechanism.[8,76] For the ODH of ethane on oxide-supported vanadia catalysts, the interface bond, e.g. V-O-Al, was also reported to be crucial for the overall reaction mechanism.[41] Thus the rather passive role of vanadia in combination with direct support participation is in sharp contrast to catalysts with inactive support materials e.g. VO_x/SiO_2 and VO_x/Al_2O_3.

While ethane and propane ODH reactivities are known to be different, a detailed experimental characterization of intermediate species in the course of alkane ODH will require further methodical developments. Once established possible differences in the mechanistic behavior may be accessible. Nevertheless, the present work on propane ODH and previous work on ethane ODH [16,17,27,28] underline the importance of the V-O-Ce bond for the overall reaction mechanism, thus showing mechanistic similarities for VO_x/ceria catalysts during short alkane ODH. To this end, it will be of great interest to apply the detailed nuclearity-dependent *operando* spectroscopic analysis of the (sub)surface dynamics presented in this study also to the ODH of ethane, which will allow to develop a more general mechanistic picture of alkane ODH over VO_x/ceria catalysts.

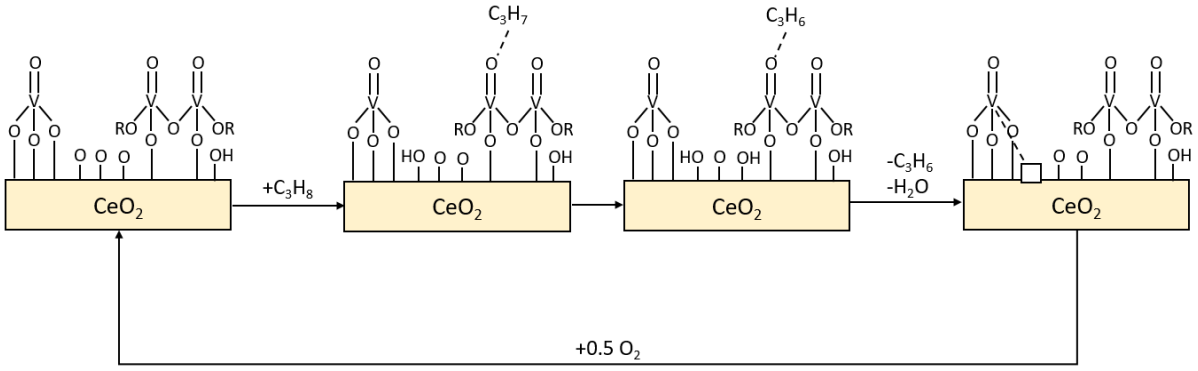

Figure 11: Proposed mechanism for propane ODH over VO_x/CeO_2 catalysts. For details see text.

4. Conclusions

In this work, we present a multiple *operando* spectroscopic study including multi-wavelength Raman, UV-Vis, and DRIFT spectroscopy for the ODH of propane on VO_x/CeO_2 catalysts. We provide direct spectroscopic evidence for the active participation of the CeO_2 support in the reaction. While the ceria surface is shown to be directly involved in the ODH reaction, the surface vanadia species are proposed to be taking part only indirectly, without observable structural changes or bond breaking. As part of the study, we have developed an experimental basis for a detailed understanding of the reaction mechanism and support participation, which may also be applied to other catalyst systems with active support materials.

Our findings show that *operando* techniques are an important tool for unravelling the dynamics in oxide catalysis with regarding to structural and electronic changes. As demonstrated for VO_x/CeO_2 catalysts, our approach allows us to disentangle the dynamics of vanadia and ceria by targeted enhancement using multi-wavelength Raman spectroscopy. Using 385 nm excitation, we were able to show that ceria is actively participating in the reaction. Thereby, hydrogen is abstracted to the ceria surface, subsequently leading to the formation of water and surface oxygen vacancies, which can interact with nearby vanadia structures. Using 514 nm excitation, we identified these structures as vanadia monomers, irreversibly blocking the defect sites and slowing down the oxygen dynamics in ceria. In addition, UV-Vis spectra revealed a redshift of the band gap energy, consistent with ceria reduction, that correlated with the conversion, further indicating the participation of ceria. The DRIFTS results provided insight into the relationship between the nature of adsorbates and catalyst selectivity, revealing that the amount of oxygen-containing adsorbates decreased sharply with increasing vanadium loading in contrast to that of oxygen-free adsorbates. This indicates that vanadia structures influence the adsorption/reaction of propane by reducing the total oxidation to CO_2.

Based on our findings, we propose a reaction mechanism for the ODH of propane over VO_x/CeO_2 catalysts. We found experimental evidence for interactions between vanadia and ceria, that had previously been observed for VO_x/CeO_2 systems [17,27,35,66] and had been described by DFT[22] but had not been verified experimentally before for propane ODH and by the applied *operando* multi-wavelength Raman, IR, and UV-Vis spectroscopies. These results go beyond previous experimental work in this area by linking the oxygen dynamics in the support material and adsorbate effects to specific vanadia structures present on the

catalyst surface (e.g. monomers interacting with oxygen vacancies). The experimental results furthermore allowed a comparison with reaction pathways for propane ODH proposed by DFT calculations, confirming the abstraction of hydrogen atoms from propane to the ceria surface rather than vanadia interface bonds.[37]

As exemplified by the VO_x/CeO_2 system, supported oxide catalysts may enable new mechanistic scenarios if active support participation is involved. In fact, in contrast to the support, vanadia is observed to participate only indirectly, i.e., no structural changes during reaction are observed, in addition to largely keeping its oxidation state at V^{5+}. This behavior may not be unique to vanadia/ceria catalysts. In fact, our approach might be expanded to other oxide catalysts with active support materials, including other transition metals (e.g. molybdena, tungstia) and/or other redox active support materials (e.g. titania). Provided the laser excitation wavelengths can be adapted to the UV-Vis properties of the catalyst, no limitations regarding the general applicability of our overall approach to a broad range of materials are expected.

Acknowledgements

The authors acknowledge Dr. Martin Brodrecht for performing nitrogen adsorption experiments and BET analysis, and Karl Kopp for technical support. This work was supported by the Deutsche Forschungsgemeinschaft (DFG, HE 4515/11-1).

Supporting Information

This information is available free of charge on the ACS Publications website. Additional Raman, UV-Vis and DRIFTS data is provided as well as further information concerning data processing and quantification.

References

[1] A.A. Ayandiran, I.A. Bakare, H. Binous, S. Al-Ghamdi, S.A. Razzak, M.M. Hossain, Oxidative dehydrogenation of propane to propylene over VO_x/CaO–γ-Al_2O_3 using lattice oxygen, Catal. Sci. Technol. 6 (2016) 5154–5167. https://doi.org/10.1039/c6cy00078a.

[2] C.A. Carrero, R. Schloegl, I.E. Wachs, R. Schomaecker, Critical Literature Review of the Kinetics for the Oxidative Dehydrogenation of Propane over Well-Defined Supported Vanadium Oxide Catalysts, ACS Catal. 4 (2014) 3357–3380. https://doi.org/10.1021/cs5003417.

[3] A.H. Elbadawi, M.S. Ba-Shammakh, S. Al-Ghamdi, S.A. Razzak, M.M. Hossain, Reduction kinetics and catalytic activity of VO_x/γ-Al_2O_3-ZrO_2 for gas phase oxygen free ODH of ethane, Chem. Eng. J. 284 (2016) 448–457. https://doi.org/10.1016/j.cej.2015.08.048.

[4] P. Hellier, P.P. Wells, D. Gianolio, M. Bowker, VO_x/Fe_2O_3 Shell-Core Catalysts for the Selective Oxidation of Methanol to Formaldehyde, Top. Catal. 61 (2018) 357–364. https://doi.org/10.1007/s11244-017-0873-2.

[5] P. Ober, S. Rogg, C. Hess, Direct Evidence for Active Support Participation in Oxide Catalysis: Multiple Operando Spectroscopy of VO_x/Ceria, ACS Catal. 10 (2020) 2999–3008. https://doi.org/10.1021/acscatal.9b05174.

[6] I. Amghizar, L.A. Vandewalle, K.M. van Geem, G.B. Marin, New Trends in Olefin Production, Engineering 3 (2017) 171–178. https://doi.org/10.1016/J.ENG.2017.02.006.

[7] F. Cavani, N. Ballarini, A. Cericola, Oxidative dehydrogenation of ethane and propane: How far from commercial implementation?, Catal. Today 127 (2007) 113–131. https://doi.org/10.1016/j.cattod.2007.05.009.

[8] B. Beck, M. Harth, N.G. Hamilton, C. Carrero, J.J. Uhlrich, A. Trunschke, S. Shaikhutdinov, H. Schubert, H.-J. Freund, R. Schlögl, J. Sauer, R. Schomäcker, Partial oxidation of ethanol on vanadia catalysts on supporting oxides with different redox properties compared to propane, J. Catal. 296 (2012) 120–131. https://doi.org/10.1016/j.jcat.2012.09.008.

[9] A. Dinse, B. Frank, C. Hess, D. Habel, R. Schomäcker, Oxidative dehydrogenation of propane over low-loaded vanadia catalysts: Impact of the support material on kinetics and selectivity, J. Mol. Catal. A Chem. 289 (2008) 28–37. https://doi.org/10.1016/j.molcata.2008.04.007.

[10] R. Bulánek, P. Čičmanec, M. Setnička, Possibility of VO_x/SiO_2 Complexes Speciation: Comparative Multi-wavelength Raman and DR UV-vis Study, Phys. Procedia 44 (2013) 195–205. https://doi.org/10.1016/j.phpro.2013.04.024.

[11] R. Grabowski, J. Słoczyński, Kinetics of oxidative dehydrogenation of propane and ethane on VO_x/SiO_2 pure and with potassium additive, Chem. Eng. Process. 44 (2005) 1082–1093. https://doi.org/10.1016/j.cep.2005.03.002.

[12] M. Piumetti, M. Armandi, E. Garrone, B. Bonelli, An IR spectroscopy assessment of the surface acidity of mesoporous VO_x–SiO_2 catalysts, Micropor. Mesopor. Mat. 164 (2012) 111–119. https://doi.org/10.1016/j.micromeso.2012.05.041.

[13] K. Shimura, T. Fujitani, Effects of promoters on the performance of a VO_x/SiO_2 catalyst for the oxidation of methane to formaldehyde, Appl. Catal. A Gen. 577 (2019) 44–51. https://doi.org/10.1016/j.apcata.2019.03.014.

[14] P. Waleska, S. Rupp, C. Hess, Operando Multiwavelength and Time-Resolved Raman Spectroscopy: Structural Dynamics of a Supported Vanadia Catalyst at Work, J. Phys. Chem. C 122 (2018) 3386–3400. https://doi.org/10.1021/acs.jpcc.7b10518.

[15] H. Zhu, S. Ould-Chikh, H. Dong, I. Llorens, Y. Saih, D.H. Anjum, J.-L. Hazemann, J.-M. Basset, VO_x/SiO_2 Catalyst Prepared by Grafting $VOCl_3$ on Silica for Oxidative Dehydrogenation of Propane, ChemCatChem 7 (2015) 3332–3339. https://doi.org/10.1002/cctc.201500607.

[16] M. Martínez-Huerta, Nature of the vanadia-ceria interface in V^{5+}/CeO_2 catalysts and its relevance for the solid-state reaction toward $CeVO_4$ and catalytic properties, J. Catal. 225 (2004) 240–248. https://doi.org/10.1016/j.jcat.2004.04.005.

[17] M.V. Martínez-Huerta, G. Deo, J.L.G. Fierro, M.A. Bañares, Operando Raman-GC Study on the Structure−Activity Relationships in V^{5+}/CeO_2 Catalyst for Ethane Oxidative

Dehydrogenation: The Formation of $CeVO_4$, J. Phys. Chem. C 112 (2008) 11441–11447. https://doi.org/10.1021/jp802827t.

[18] M.A. Bañares, I.E. Wachs, Molecular structures of supported metal oxide catalysts under different environments, J. Raman Spectrosc. 33 (2002) 359–380. https://doi.org/10.1002/jrs.866.

[19] M.V. Ganduglia-Pirovano, C. Popa, J. Sauer, H. Abbott, A. Uhl, M. Baron, D. Stacchiola, O. Bondarchuk, S. Shaikhutdinov, H.-J. Freund, Role of ceria in oxidative dehydrogenation on supported vanadia catalysts, J. Am. Chem. Soc. 132 (2010) 2345–2349. https://doi.org/10.1021/ja910574h.

[20] Z. Hu, Z. Wang, Y. Guo, L. Wang, Y. Guo, J. Zhang, W. Zhan, Total Oxidation of Propane over a Ru/CeO_2 Catalyst at Low Temperature, Environ. Sci. 52 (2018) 9531–9541. https://doi.org/10.1021/acs.est.8b03448.

[21] Y. Li, Z. Wei, F. Gao, L. Kovarik, R.A.L. Baylon, C.H.F. Peden, Y. Wang, Effect of Oxygen Defects on the Catalytic Performance of VO_x/CeO_2 Catalysts for Oxidative Dehydrogenation of Methanol, ACS Catal. 5 (2015) 3006–3012. https://doi.org/10.1021/cs502084g.

[22] C. Penschke, J. Paier, J. Sauer, Oligomeric Vanadium Oxide Species Supported on the CeO_2 (111) Surface: Structure and Reactivity Studied by Density Functional Theory, J. Phys. Chem. C 117 (2013) 5274–5285. https://doi.org/10.1021/jp400520j.

[23] C. Penschke, J. Paier, J. Sauer, Vanadium Oxide Oligomers and Ordered Monolayers Supported on CeO_2 (111): Structure and Stability Studied by Density Functional Theory, J. Phys. Chem. C 122 (2018) 9101–9110. https://doi.org/10.1021/acs.jpcc.8b01998.

[24] C. Popa, M.V. Ganduglia-Pirovano, J. Sauer, Periodic Density Functional Theory Study of VO n Species Supported on the CeO_2 (111) Surface, J. Phys. Chem. C 115 (2011) 7399–7410. https://doi.org/10.1021/jp108185y.

[25] M.N. Taylor, A.F. Carley, T.E. Davies, S.H. Taylor, The Oxidative Dehydrogenation of Propane Using Vanadium Oxide Supported on Nanocrystalline Ceria, Top. Catal. 52 (2009) 1660–1668. https://doi.org/10.1007/s11244-009-9307-0.

[26] X.-P. Wu, J. Liu, J. Fan, X.-Q. Gong, Theoretical studies on the monomeric vanadium oxides supported by ceria: the atomic structures and oxidative dehydrogenation activities, RSC Adv. 5 (2015) 52259–52263. https://doi.org/10.1039/c5ra08962j.

[27] A. Iglesias-Juez, M.V. Martínez-Huerta, E. Rojas-García, J.-M. Jehng, M.A. Bañares, On the Nature of the Unusual Redox Cycle at the Vanadia Ceria Interface, J. Phys. Chem. C 122 (2018) 1197–1205. https://doi.org/10.1021/acs.jpcc.7b09832.

[28] M.V. Martínez-Huerta, G. Deo, J.L.G. Fierro, M.A. Bañares, Changes in Ceria-Supported Vanadium Oxide Catalysts during the Oxidative Dehydrogenation of Ethane and Temperature-Programmed Treatments, J. Phys. Chem. C 111 (2007) 18708–18714. https://doi.org/10.1021/jp0772225.

[29] X. Gao, M.A. Bañares, I.E. Wachs, Ethane and n-Butane Oxidation over Supported Vanadium Oxide Catalysts: An in Situ UV–Visible Diffuse Reflectance Spectroscopic Investigation, J. Catal. 188 (1999) 325–331. https://doi.org/10.1006/jcat.1999.2647.

[30] M.O. Guerrero-Pérez, A.J. McCue, J.A. Anderson, Rapid scan FTIR reveals propane (am)oxidation mechanisms over vanadium based catalysts, J. Catal. 390 (2020) 72–80. https://doi.org/10.1016/j.jcat.2020.07.031.

[31] J.J. Ternero-Hidalgo, M.O. Guerrero-Pérez, J. Rodríguez-Mirasol, T. Cordero, M.A. Bañares, R. Portela, P. Bazin, G. Clet, M. Daturi, Operando Reactor-Cell with Simultaneous Transmission FTIR and Raman Characterization (IRRaman) for the Study of Gas-Phase Reactions with Solid Catalysts, Anal. Chem. 92 (2020) 5100–5106. https://doi.org/10.1021/acs.analchem.9b05473.

[32] M.A. Bañares, M.V. Martínez-Huerta, X. Gao, J.L.G. Fierro, I.E. Wachs, Dynamic behavior of supported vanadia catalysts in the selective oxidation of ethane, Catal. Today 61 (2000) 295–301. https://doi.org/10.1016/S0920-5861(00)00388-6.

[33] M.A. Bañares, M. Martínez-Huerta, X. Gao, I.E. Wachs, J.L.G. Fierro, Identification and roles of the different active sites in supported vanadia catalysts by in situ techniques, in: 12th International Congress on Catalysis, Proceedings of the 12th ICC, Elsevier, 2000, pp. 3125–3130.

[34] Z. Wu, Multi-wavelength Raman spectroscopy study of supported vanadia catalysts: Structure identification and quantification, Chin. J. Catal. 35 (2014) 1591–1608. https://doi.org/10.1016/S1872- 2067(14)60082- 6.

[35] Z. Wu, A.J. Rondinone, I.N. Ivanov, S.H. Overbury, Structure of Vanadium Oxide Supported on Ceria by Multiwavelength Raman Spectroscopy, J. Phys. Chem. C 115 (2011) 25368–25378. https://doi.org/10.1021/jp2084605.

[36] T. Kropp, J. Paier, J. Sauer, Support effect in oxide catalysis: methanol oxidation on vanadia/ceria, J. Am. Chem. Soc. 136 (2014) 14616–14625. https://doi.org/10.1021/ja508657c.

[37] C. Huang, Z.-Q. Wang, X.-Q. Gong, Activity and selectivity of propane oxidative dehydrogenation over VO_3/CeO_2 (111) catalysts: A density functional theory study, Chin. J. Catal. 39 (2018) 1520–1526. https://doi.org/10.1016/S1872-2067(18)63072-4.

[38] X.-P. Wu, X.-Q. Gong, Unique Electronic and Structural Effects in Vanadia/Ceria-Catalyzed Reactions, J. Am. Chem. Soc. 137 (2015) 13228–13231. https://doi.org/10.1021/jacs.5b07939.

[39] Z. Hu, X. Liu, D. Meng, Y. Guo, Y. Guo, G. Lu, Effect of Ceria Crystal Plane on the Physicochemical and Catalytic Properties of Pd/Ceria for CO and Propane Oxidation, ACS Catal. 6 (2016) 2265–2279. https://doi.org/10.1021/acscatal.5b02617.

[40] Y. Li, Z. Wei, F. Gao, L. Kovarik, C.H.F. Peden, Y. Wang, Effects of CeO_2 support facets on VO_x/CeO_2 catalysts in oxidative dehydrogenation of methanol, J. Catal. 315 (2014) 15–24. https://doi.org/10.1016/j.jcat.2014.04.013.

[41] M. Martínez-Huerta, X. Gao, H. Tian, I. Wachs, J. Fierro, M. Banares, Oxidative dehydrogenation of ethane to ethylene over alumina-supported vanadium oxide catalysts: Relationship between molecular structures and chemical reactivity, Catal. Today 118 (2006) 279–287. https://doi.org/10.1016/j.cattod.2006.07.034.

[42] A. Klisińska, K. Samson, I. Gressel, B. Grzybowska, Effect of additives on properties of V_2O_5/SiO_2 and V_2O_5/MgO catalysts, Appl. Catal. A Gen. 309 (2006) 10–16. https://doi.org/10.1016/j.apcata.2006.04.028.

[43] A. Kubas, J. Noak, A. Trunschke, R. Schlögl, F. Neese, D. Maganas, A combined experimental and theoretical spectroscopic protocol for determination of the structure of heterogeneous catalysts: developing the information content of the resonance Raman spectra of M1 $MoVO_x$, Chem. Sci. 8 (2017) 6338–6353. https://doi.org/10.1039/C7SC01771E.

[44] A. Filtschew, K. Hofmann, C. Hess, Ceria and Its Defect Structure: New Insights from a Combined Spectroscopic Approach, J. Phys. Chem. C 120 (2016) 6694–6703. https://doi.org/10.1021/acs.jpcc.6b00959.

[45] P.S. Waleska, C. Hess, Oligomerization of Supported Vanadia: Structural Insight Using Surface-Science Models with Chemical Complexity, J. Phys. Chem. C 120 (2016) 18510–18519. https://doi.org/10.1021/acs.jpcc.6b01672.

[46] A.A. Vikharev, G.G. Denisov, V.V. Kocharovsky, S.V. Kuzikov, V.V. Parshin, N.Y. Peskov, A.N. Stepanov, D.I. Sobolev, M.Y. Shmelev, Fast quasi-optical phase shifter based on the effect of induced photo conductivity in silicon, Radiophys. Quantum Electr. 50 (2007) 786–793. https://doi.org/10.1007/s11141-007-0069-x.

[47] I.E. Paulauskas, G.E. Jellison, L.A. Boatner, G.M. Brown, Photoelectrochemical Stability and Alteration Products of n-Type Single-Crystal ZnO Photoanodes, Intern. J. Electrochem. 2011 (2011) 1–10. https://doi.org/10.4061/2011/563427.

[48] J. Kreisel, M.C. Weber, N. Dix, F. Sánchez, P.A. Thomas, J. Fontcuberta, Probing Individual Layers in Functional Oxide Multilayers by Wavelength-Dependent Raman Scattering, Adv. Funct. Mater. 22 (2012) 5044–5049. https://doi.org/10.1002/adfm.201201272.

[49] B. Huang, R. Gillen, J. Robertson, Study of CeO_2 and Its Native Defects by Density Functional Theory with Repulsive Potential, J. Phys. Chem. C 118 (2014) 24248–24256. https://doi.org/10.1021/jp506625h.

[50] M. Lohrenscheit, C. Hess, Direct Evidence for the Participation of Oxygen Vacancies in the Oxidation of Carbon Monoxide over Ceria-Supported Gold Catalysts by using Operando Raman Spectroscopy, ChemCatChem 8 (2016) 523–526. https://doi.org/10.1002/cctc.201501129.

[51] C. Schilling, C. Hess, Real-Time Observation of the Defect Dynamics in Working Au/CeO_2 Catalysts by Combined Operando Raman/UV–Vis Spectroscopy, J. Phys. Chem. C 122 (2018) 2909–2917. https://doi.org/10.1021/acs.jpcc.8b00027.

[52] D. Nitsche, C. Hess, Structure of Isolated Vanadia and Titania: A Deep UV Raman, UV–Vis, and IR Spectroscopic Study, J. Phys. Chem. C 120 (2016) 1025–1037. https://doi.org/10.1021/acs.jpcc.5b10317.

[53] C. Schilling, A. Hofmann, C. Hess, M.V. Ganduglia-Pirovano, Raman Spectra of Polycrystalline CeO_2 A Density Functional Theory Study, J. Phys. Chem. C 121 (2017) 20834–20849. https://doi.org/10.1021/acs.jpcc.7b06643.

[54] Z. Wu, M. Li, J. Howe, H.M. Meyer, S.H. Overbury, Probing defect sites on CeO_2 nanocrystals with well-defined surface planes by Raman spectroscopy and O_2 adsorption, Langmuir 26 (2010) 16595–16606. https://doi.org/10.1021/la101723w.

[55] J.-M. Jehng, G. Deo, B.M. Weckhuysen, I.E. Wachs, Effect of water vapor on the molecular structures of supported vanadium oxide catalysts at elevated temperatures, J. Mol. Catal. A Chem. 110 (1996) 41–54. https://doi.org/10.1016/1381-1169(96)00061-1.

[56] M. Baron, H. Abbott, O. Bondarchuk, D. Stacchiola, A. Uhl, S. Shaikhutdinov, H.-J. Freund, C. Popa, M.V. Ganduglia-Pirovano, J. Sauer, Resolving the atomic structure of vanadia monolayer catalysts: monomers, trimers, and oligomers on ceria, Angew. Chem. Int. Ed. 48 (2009) 8006–8009. https://doi.org/10.1002/anie.200903085.

[57] W. Daniell, A. Ponchel, S. Kuba, F. Anderle, T. Weingand, D.H. Gregory, H. Knözinger, Characterization and Catalytic Behavior of VO_x-CeO_2 Catalysts for the Oxidative Dehydrogenation of Propane, Top. Catal. 20 (2002) 65–74. https://doi.org/10.1023/A:1016399315511.

[58] P. Gruene, T. Wolfram, K. Pelzer, R. Schlögl, A. Trunschke, Role of dispersion of vanadia on SBA-15 in the oxidative dehydrogenation of propane, Catal. Today 157 (2010) 137–142. https://doi.org/10.1016/j.cattod.2010.03.014.

[59] M.L. Peña, A. Dejoz, V. Fornés, F. Rey, M.I. Vázquez, J.M. López Nieto, V-containing MCM-41 and MCM-48 catalysts for the selective oxidation of propane in gas phase,

Appl. Catal. A Gen. 209 (2001) 155–164. https://doi.org/10.1016/S0926-860X(00)00761-4.

[60] J. LIU, Z. ZHAO, C. XU, A. DUAN, G. JIANG, CeO_2-supported vanadium oxide catalysts for soot oxidation: the roles of molecular structure and nanometer effect, J. Rare Earths 28 (2010) 198–204. https://doi.org/10.1016/S1002-0721(09)60080-6.

[61] R.J. Deeth, Electronic structures and d-d spectra of vanadium(IV) and VO^{2+} complexes: discrete variational Xα calculations, J. Chem. Soc., Dalton Trans. 65 (1991) 1467–1477. https://doi.org/10.1039/DT9910001467.

[62] N.V. Skorodumova, R. Ahuja, S.I. Simak, I.A. Abrikosov, B. Johansson, B.I. Lundqvist, Electronic, bonding, and optical properties of CeO_2 and Ce_2O_3 from first principles, Phys. Rev. B 64 (2001) 548. https://doi.org/10.1103/PhysRevB.64.115108.

[63] X. Gao, J.-M. Jehng, I.E. Wachs, In Situ UV–vis–NIR Diffuse Reflectance and Raman Spectroscopic Studies of Propane Oxidation over ZrO_2-Supported Vanadium Oxide Catalysts, J. Catal. 209 (2002) 43–50. https://doi.org/10.1006/jcat.2002.3635.

[64] Z. Zhao, Y. Yamada, A. Ueda, H. Sakurai, T. Kobayashi, The roles of redox and acid–base properties of silica-supported vanadia catalysts in the selective oxidation of ethane, Catal. Today 93-95 (2004) 163–171. https://doi.org/10.1016/j.cattod.2004.06.130.

[65] A. Abd El-Moemen, A.M. Abdel-Mageed, J. Bansmann, M. Parlinska-Wojtan, R.J. Behm, G. Kučerová, Deactivation of Au/CeO_2 catalysts during CO oxidation: Influence of pretreatment and reaction conditions, J. Catal. 341 (2016) 160–179. https://doi.org/10.1016/j.jcat.2016.07.005.

[66] A. Badri, C. Binet, J.-C. Lavalley, An FTIR study of surface ceria hydroxy groups during a redox process with H_2, Faraday Trans. 92 (1996) 4669. https://doi.org/10.1039/FT9969204669.

[67] M.A. Centeno, I. Carrizosa, J.A. Odriozola, NO–NH_3 coadsorption on vanadia/titania catalysts: determination of the reduction degree of vanadium, Appl. Catal. B 29 (2001) 307–314. https://doi.org/10.1016/S0926-3373(00)00214-9.

[68] L. Friedman, J. Turkevich, The Infra- Red Absorption Spectra of Propane- D-1 and Propane- D-2, Int. J. Chem. Phys. 17 (1949) 1012–1015. https://doi.org/10.1063/1.1747105.

[69] C. Binet, M. Daturi, J.-C. Lavalley, IR study of polycrystalline ceria properties in oxidised and reduced states, Catal. Today 50 (1999) 207–225. https://doi.org/10.1016/S0920-5861(98)00504-5.

[70] C. Li, Y. Sakata, T. Arai, K. Domen, K.-i. Maruya, T. Onishi, Carbon monoxide and carbon dioxide adsorption on cerium oxide studied by Fourier-transform infrared spectroscopy. Part 1.-Formation of carbonate species on dehydroxylated CeO_2, at room temperature, J. Chem. Soc., Faraday Trans. 1 85 (1989) 929. https://doi.org/10.1039/F19898500929.

[71] C. Schilling, C. Hess, Elucidating the Role of Support Oxygen in the Water–Gas Shift Reaction over Ceria-Supported Gold Catalysts Using Operando Spectroscopy, ACS Catal. 9 (2019) 1159–1171. https://doi.org/10.1021/acscatal.8b04536.

[72] G.N. Vayssilov, M. Mihaylov, P. St. Petkov, K.I. Hadjiivanov, K.M. Neyman, Reassignment of the Vibrational Spectra of Carbonates, Formates, and Related Surface Species on Ceria: A Combined Density Functional and Infrared Spectroscopy Investigation, J. Phys. Chem. C 115 (2011) 23435–23454. https://doi.org/10.1021/jp208050a.

[73] A. Badri, C. Binet, J.-C. Lavalley, Surface-Chlorinated Ceria and Chlorine-Containing Reduced Pd/CeO_2 Catalysts. A FTIR Study, J. Phys. Chem. 100 (1996) 8363–8368. https://doi.org/10.1021/jp953023m.

[74] D. Shee, G. Deo, Adsorption and ODH reaction of alkane on sol–gel synthesized TiO_2–WO_3 supported vanadium oxide catalysts: In situ DRIFT and structure–reactivity study, J. Mol. Catal. A Chem. 308 (2009) 46–55. https://doi.org/10.1016/j.molcata.2009.03.032.

[75] K. Chen, A.T. Bell, E. Iglesia, Kinetics and Mechanism of Oxidative Dehydrogenation of Propane on Vanadium, Molybdenum, and Tungsten Oxides, J. Phys. Chem. B 104 (2000) 1292–1299. https://doi.org/10.1021/jp9933875.

[76] M.M. Hossain, Kinetics of Oxidative Dehydrogenation of Propane to Propylene Using Lattice Oxygen of $VO_x/CaO/\gamma\text{-}Al_2O_3$ Catalysts, Ind. Eng. Chem. Res. 56 (2017) 4309–4318. https://doi.org/10.1021/acs.iecr.7b00759.